10-1-2004

Laboratory and Field Fatigue Investigation of Cantilevered Signal Support Structures in the City of Philadelphia

Ian C. Hodgson

Robert J. Connor

John Hall

Carl Bowman

LABORATORY AND FIELD FATIGUE INVESTIGATION OF CANTILEVERED SIGNAL SUPPORT STRUCTURES IN THE CITY OF PHILADELPHIA

by

Robert J. Connor

Ian C. Hodgson

John Hall

Carl Bowman

FINAL REPORT

ATLSS Report No. 04-22

October 2004

ATLSS is a National Center for Engineering Research on Advanced Technology for Large Structural Systems

117 ATLSS Drive
Bethlehem, PA 18015-4729

Phone: (610)758-3525
Fax: (610)758-5902

www.atlss.lehigh.edu
Email: inatl@lehigh.edu

LABORATORY AND FIELD FATIGUE INVESTIGATION OF CANTILEVERED SIGNAL SUPPORT STRUCTURES IN THE CITY OF PHILADELPHIA

by

Robert J. Connor
Research Engineer
ATLSS Engineering Research Center

Ian C. Hodgson
Research Engineer
ATLSS Engineering Research Center

John Hall
Graduate Research Assistant
ATLSS Engineering Research Center

Carl Bowman
Instrumentation Technician
ATLSS Engineering Research Center

FINAL REPORT

ATLSS Report No. 04-22

October 2004

ATLSS is a National Center for Engineering Research on Advanced Technology for Large Structural Systems

117 ATLSS Drive
Bethlehem, PA 18015-4729

Phone: (610)758-3525
Fax: (610)758-5902

www.atlss.lehigh.edu
Email: inatl@lehigh.edu

Table of Contents

1.0 Introduction

This Final Report discusses and summarizes the initial results of the field testing and monitoring of selected cantilevered mast-arm signal structures in Philadelphia, PA. This work was conducted as part of a comprehensive inspection and fatigue evaluation project under the direction of Edwards and Kelcey, consulting engineers.

In order to better define the potential level of fatigue damage due to natural wind, a field instrumentation and remote monitoring program was developed and implemented. The program included static controlled load tests on two cantilevered mast-arm structures in order to establish the global response of the structures to known loads. Valuable information pertaining to actual stress distributions at fatigue critical details, such as the column-to-base plate connection, was obtained. Dynamic tests were conducted in order to determine the natural frequency, vibration characteristics, and the amount of damping in the structures.

In addition, remote long-term monitoring of these structures is underway in order to develop stress-range histograms at critical details. The monitoring was performed between April 1, 2002 and January 3, 2003, for a total of eight months. The two structures were located in areas determined by the City to be most susceptible to high wind conditions. The first structure is located adjacent to the Philadelphia International Airport at the southeast corner of the intersection of Industrial Highway (SR291) and Island Avenue, as shown in Figure 1.1. The second structure is located at the southeast corner of the intersection of Lindbergh Boulevard and 84th Street. The two structures are similar in construction and configuration. Figure 1.2 contains an aerial view of the two structures. Triggered time history records, stress-range histograms, and wind speed histograms were developed.

Figure 1.1 – Photograph of mast-arm structure being monitored
(Structure at Industrial Highway (SR291) and Island Avenue shown)

Figure 1.2 – Aerial photograph of the two mast-arm structures being monitored
(Note orientation of mast-arm illustrated on photograph)

2.0 Instrumentation Plan and Data Acquisition

The following section describes the sensors and instrumentation plan used during the field testing and monitoring program. "As built" instrumentation plans detailing the locations of all sensors installed on both structures are provided in Appendix A

2.1 Strain Gages

Strain gages were placed at locations known to be fatigue sensitive and/or to provide global load distribution characteristics of the structure.

All strain gages installed in the field were produced by Measurements Group Inc. and were 0.25 in. gage length type LWK-06-W250B-350. These are a uniaxial weldable resistance strain gage. Weldable type strain gages were selected due to ease of installation in a variety of weather conditions. The "welds" are a point or spot resistance weld about the size of a pin prick. The probe is powered by a battery and only touches the foil that the strain gage is mounted on by the manufacturer. This fuses a small pin size area to the steel surface. It takes forty or more of these dots to attach the gage to the steel surface. There are no arc strikes or heat affected zones that are discernible. There is no preheat or any other preparation involved other than the preparation of the local metal surface by grinding and then cleaning before the gage is attached to the component with the welding unit. There has never been an instance of adverse behavior associated with the use of weldable strain gages including their installation on extremely brittle material such as A615 Gr75 steel reinforcing bars.

These gages are a temperature-compensated uniaxial strain gage and perform very well when accurate strain measurements are required over long periods of time (months to years). The gage resistance was 350Ω and an excitation voltage of 10 Volts was used. The gages where installed at locations where access was good and the effects of very high strain gradients were not a concern.

All gages were protected with a multi-layer system and then sealed with a silicon type agent. Where required, wire connections were soldered and electrically insulated with heat shrink tube.

2.2 Summary of Sensor Installations

The following section summarizes the strain gage plan. The detailed gage plan, showing the locations of all gages is provided in Appendix A.

2.2.1 Gages on Mast-arm

Strain gages were installed on the cantilevered mast-arm at the connection to the column. Figure 2.1 illustrates a typical installation of these gages prior to fully securing the wires for the long-term monitoring program. Gages were installed at the 6, 9, 12, and 3-O'clock positions on the mast-arm. These gages were installed on the primary geometric axis of the mast-arm in order measure primary bending stresses. In addition, two gages were installed in-line with the upper bolts in the flange plates, as shown in Figure 2.1. These gages were installed to determine the potential stress increase in the tube wall adjacent to the bolts due to flexibility of the flange plate. All gages were installed 4" from the flange plate.

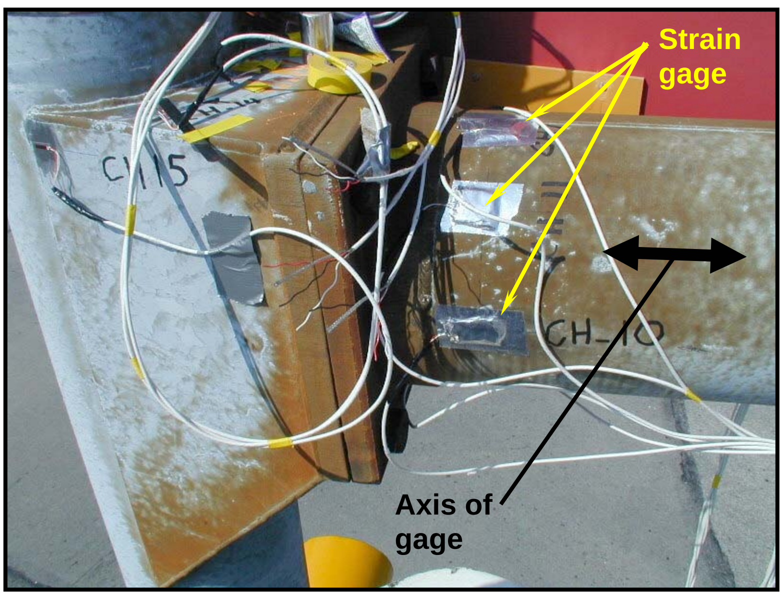

Figure 2.1 - Photograph of strain gages on mast-arm at connection of mast-arm to column flange plate. Note gage in-line with upper near anchor rod (CH_11)

2.2.2 Gages on Column

Uniaxial strain gages were installed on the column near the base plate as shown in Figures 2.2. Similar to the mast-arm, strain gages were installed on the primary geometric axis of the mast-arm in order measure primary bending stresses. In addition, two gages were installed in line with the rear anchor rods, as shown in Figure 2.2 (*Note position of channel CH_6 in Figure 2.2*). These gages were installed to determine the potential stress increase in the tube wall adjacent to the bolts due to flexibility of the base plate. Previous testing and analysis conducted by the researchers has demonstrated that base plate flexibility can significantly alter the stresses in the anchor rods and pole near the connection. All gages were installed 4 inches from the base plate.

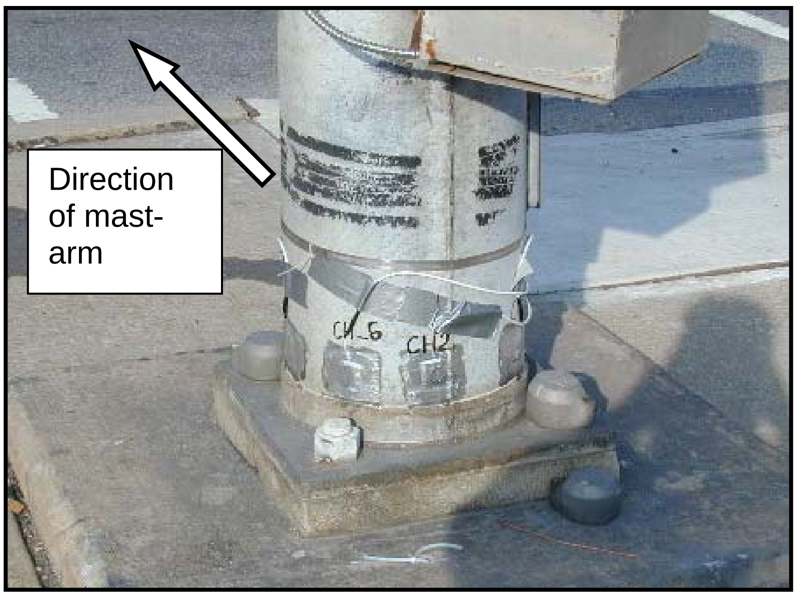

Figure 2.2 - Photograph of strain gages at column base.
Note gage in-line with near left anchor rod (CH_6)

2.2.3 Gages on Flange Connection Plates at Top of Pole

Gages were installed at selected locations on the plates that connect the pole flange plate to the pole. These plates are indicated in Figure 2.3. Strain gages were installed immediately adjacent to the toe of the weld that connects the plates to the tube wall. Note that the gages on the top plate are oriented perpendicular to the weld toe (*note that only one of these gages are visible in the photograph*). Fatigue cracks would be expected to originate perpendicular the weld toe at these locations. Hence, the stress range of interest should be determined (i.e., measured or calculated) perpendicular to the weld toe. Gages were only installed at these locations on the pole located at 84th and Lindbergh.

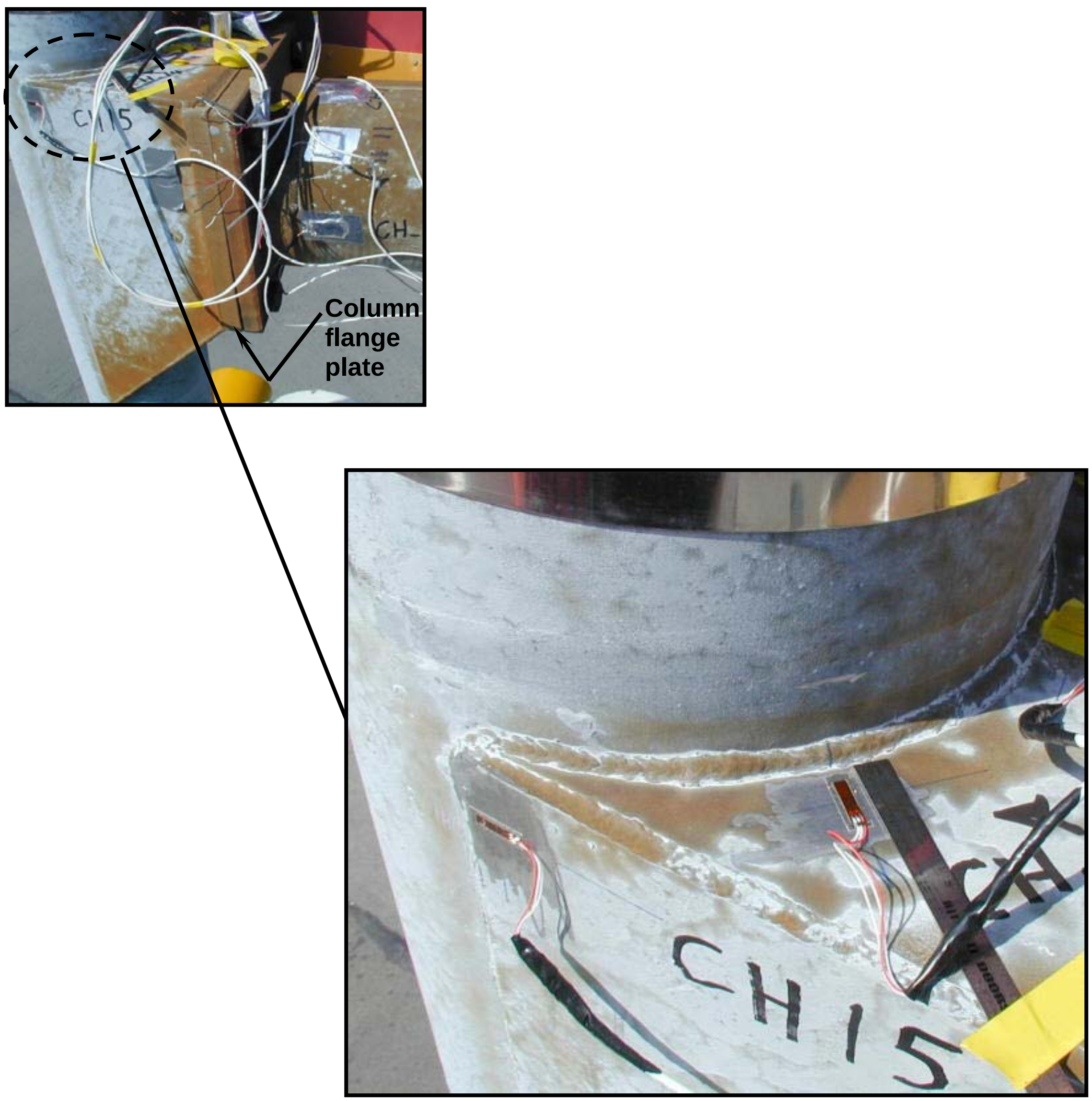

Figure 2.3 - Photograph of strain gages on plates connecting flange plate to pole (84th and Lindbergh only)

2.2.4 Accelerometer Installed at Tip of Mast-Arm

A single tri-axial piezoelectric accelerometer was mounted to the tip of each mast-arm for all tests controlled load tests and during the long-term monitoring program. The accelerometer is model number CXL100HF3 manufactured by Crossbow Technology, Inc. This sensor has an input range of ±100 g, and a frequency bandwidth of 0.3 to 1000 Hz.

Displacements at the tip of the mast-arm were determined by integrating the acceleration records twice. Before each integration, the data were high-pass filtered to remove unwanted drift in the calculated results. A comparison between measured and calculated displacements was performed and will be discussed.

2.2.5 Displacement Sensor at Tip of Mast-Arm

During some of the static and dynamic load tests, a string pot was connected to the tip of the mast-arm to measure vertical displacements of the mast-arm with respect to ground, which required closure of the lane beneath the tip of the mast-arm. The string pot is a linear motion transducer, manufactured by Patriot Systems, model number P-20A. This sensor has a displacement capacity of 20 inches.

2.2.6 Anemometer

An anemometer was installed at the top of each pole in order to measured wind speed and direction. Figure 2.4 is a photograph of the anemometer installed at the 84th and Lindbergh site. The units are rugged high-performance wind sensors manufacture by R.M. Young Company of Traverse City, Michigan. Model 05103 was selected for this application and is capable of measuring wind speeds of up to 134 mph.

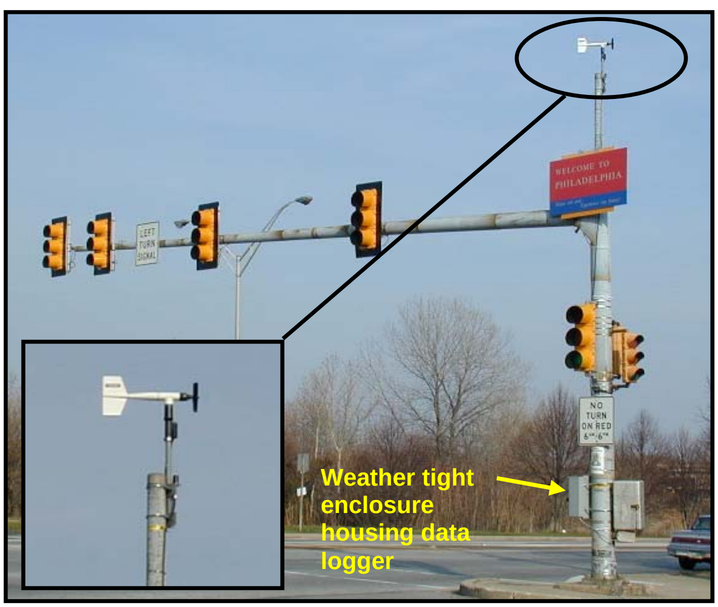

Figure 2.4 – Photograph of anemometer installed at 84th and Lindbergh structure (Island Avenue installation similar)

2.3 Data Acquisition

2.3.1 On-site Controlled Testing

Data were collected using a Campbell Scientific CR9000 Data Logger. This is a high speed, multi-channel, 16-bit digital data acquisition system. The sampling rate was 250Hz during the on-site testing. In order to ensure a stable, noise-free signal, analog and digital filtering were employed. Using a laptop computer, real-time review of the data was possible during all tests. Hence, sensors could be checked in real-time to ensure proper operation.

While on site, power was provided by generators or directly from the power source used to operate the signals.

2.3.2 Remote Long-term Monitoring

Remote long-term monitoring of selected gages was conducted using a CR5000 Data Logger, also manufactured by Campbell Scientific. The monitoring began after an initial review of the measurements taken during the controlled static and dynamic tests was completed. The data logger was stored in a weather tight enclosure mounted to the pole, as shown in Figure 2.4.

Remote communication with the CR5000 was made using a wireless CDPD modem installed at each pole. Using special software installed on a server located at the ATLSS laboratory in Bethlehem, PA, data were collected automatically. The server polled each structure at regular intervals and retrieved all current data. This automation greatly reduced the amount of time required related to the long-term monitoring effort. Power was obtained by installing an outlet in the enclosure which housed the data logger. The outlet was connected to the power source used to operate the signals and was provided by the City of Philadelphia.

3.0 Test Program - Summary

The test program included controlled load tests and uncontrolled monitoring of random wind events. These tests and the data collected are discussed below.

3.1 Controlled Load Tests

3.1.1 Static Load Tests

In order to verify the operation of the equipment, verify structural analysis models, and better understand the behavior of the structure, static load tests were conducted. These tests were conducted by suspending known loads from the tip of the cantilever mast-arm while data were collected. Stresses from all gages and tip displacement were recorded. For some tests, load was applied in steps of 25, 50, 75, and 100 lbs. Applying the load in steps verifies that the structure and instrumentation responds in a linear elastic manor. Only vertical loads could be applied in this way. The tests are summarized for both structures in Tables 3.1 and 3.2.

In order to gain some insight into the response of the pole to horizontal loading, a force was applied at the tip of the mast-arm in the horizontal plane. A wire was secured to the bucket of the man-lift and the tip of the mast-arm. The bucket was very slowly moved away from the pole in the horizontal plane perpendicular to the axis of the mast-arm. Care was taken to ensure that the force was applied perpendicular to the mast-arm. Only stresses were recorded as horizontal displacements could not be measured. Although no measure of the applied load was made, these tests provide valuable data related to the behavior of the structure when subjected to a static horizontal load. These data will be useful when estimating applied horizontal wind forces.

3.1.2 Dynamic Load Tests

It is well known that cantilevered mast-arm structures possess very little damping. Once excited by natural wind gusts, similar structures have been observed to oscillate freely, accumulating many stress cycles. To establish the amount of damping in the structures being monitored, dynamic tests were conducted at both locations. The tests are summarized for both structures in Tables 3.1 and 3.2.

For the vertical vibration tests, a known force was applied at the tip of the mast-arm by suspending a 100 lb weight from a thin wire. After the weight was suspended and the pole was at static equilibrium, the wire was cut and the pole was permitted to vibrate freely for several minutes while data were recorded. Data were collected from all strain gages, the tri-axial accelerometer, and the displacement sensor.

The data will be used to determine the natural frequency of the structure and the modes of vibration, the damping characteristics, and the dominant mode of vibration. As stated above, displacements can be calculated by integrating the acceleration data twice. Since displacements were directly measured, the displacements calculated using the acceleration data could be compare to the measured data.

As discussed, these structures are known to be very lightly damped. The displacement sensor housing rests on the ground and attaches to the tip of the mast-arm using a long wire. To maintain tension on the wire, a spring in built into the sensor housing. Tests conducted at Texas Tech have suggested that this type of sensor (*i.e., spring loaded*) may add to the damping of these structures and therefore alter the observed dynamic behavior. In order to further investigate this observation and determine the effect, if any, on the poles under study, the tests were conducted with and without the displacement sensor wire connected to the tip of the mast-arm. Data were recorded from the strain gages and the triaxial accelerometer.

Tests were also conducted in the horizontal direction by applying a horizontal force as described above. The force was released instantaneously by cutting a wire attached to the tip of the mast-arm and the bucket of the man-lift. The data from the stain gages and accelerometer were recorded.

Test #	File Name[2]	Direction of Load	Load (lbs)	String pot Attached	Comments
1	T84_25_1.DAT	Vertical	25	Yes	Very windy & cold
2	T84_100_1.DAT	Vertical	100	Yes	Very windy & cold
3	T84_100_2.DAT	Vertical	100	Yes	Very windy & cold
4	T84_100_3.DAT	Vertical	100	No	Very windy & cold
5	T84_100_4.DAT	Vertical	100	No	Very windy & cold
6	T84_H1.DAT	Horizontal	*See Note 1*	No	Very windy & cold - The wire connected to the mast-arm was pulled by hand
7	T84_H2.DAT	Horizontal		No	

Notes:
1. Load was applied horizontally by pulling on wire attached to the pole from the man lift.
2. Static and dynamic test. Dynamic tests were conducted by cutting wire used to apply load.

Table 3.1 - Summary of controlled tests conduct at pole located at 84th and Lindbergh

Test #	File Name[2]	Direction of Load	Load (lbs)	String pot Attached	Comments
1	ISL_250A.DAT	Vertical	100	Yes	Very Windy
2	ISL_250B.DAT	Vertical	100	Yes	Very Windy
3	ISL_250C.DAT	Vertical	100	Yes	Light Wind
4	ISL_250D.DAT	Vertical	100	Yes	Windy
5	ISL_250E.DAT	Vertical	100	Yes	Very Windy
6	ISL_250F.DAT	Vertical	100	No	Light Wind
7	ISL_250G.DAT	Vertical	100	No	Light Wind – Weight Slipped
8	ISL_250H.DAT	Vertical	100	No	Light Wind
9	ISL_250I.DAT	Horizontal	*See Note 1*	No	Windy – Pulled w/ Manlift
10	ISL_250J.DAT	Horizontal		No	Windy – Pulled w/ Manlift
11	ISL_250K.DAT	Horizontal		No	Windy – Pulled w/ Manlift

Notes:
1. Load was applied horizontally by pulling on wire attached to the pole from the man lift.
2. Static and dynamic test. Dynamic tests were conducted by cutting wire used to apply load.

Table 3.2 - Summary of controlled tests conduct at pole located at Island Ave. and SR 291

3.2 Remote Monitoring Program

The data collected during the long-term monitoring program is summarized in this section. The mast-arm structures at 84th street and Island Ave. were instrumented with 15 and 12 uniaxial strain gages, respectively. However, to reduce the amount of data collected, only critical strain gages were selected to be included in the long-term monitoring program. The accelerometer (all three axis), wind speed, and wind direction are also recorded at each structure. Tables 3.3 and 3.4 present the strain gages included in the long-term monitoring program for the Island/SR 291 and 84th/Lindbergh poles, respectively.

Monitored Channel No.	Strain Gage
1	CH_2
2	CH_3
3	CH_4
4	CH_5
5	CH_6
6	CH_7
7	CH_8
8	CH_10
9	CH_11

Table 3.3 - Summary of strain gages selected for remote long-term monitoring program for the pole located at Island Ave. and SR 291

Monitored Channel No.	Strain Gage
1	CH_2
2	CH_3
3	CH_4
4	CH_5
5	CH_6
6	CH_7
7	CH_8
8	CH_9
9	CH_10
10	CH_15

Table 3.4 - Summary of strain gages selected for remote long-term monitoring program for the pole located at 84th St. and Lindbergh Blvd.

The gages were selected after an in-depth review of the data collected during the static and dynamic controlled load tests was completed. In addition, a limited amount of data were collected from all gages as the poles were subjected to random wind. These data were collected while ATLSS personnel were on-site and remotely from Lehigh University using the wireless modems previously described. Although a reduced number of gages were monitored, the behavior of the structures can still be defined under random wind events since the response of the structure was well defined during the controlled load tests. Sufficient data are being collected in order to make an accurate fatigue damage assessment.

3.2.1 Wind Data

In order to develop an accurate estimate of the characteristics of natural wind in the area of each pole, wind speed and direction are continuously recorded at predefined intervals at each pole. The average angle of attack of the wind, the maximum winds speed, and average wind speed during the interval are recorded. These data files will be used to develop detailed wind speed/direction histograms for each location. The data can be compared with established statistical distributions and historical weather data.

3.2.2 Stress-range Histograms

Data for stress-range histograms were developed using the rainflow cycle counting method. The stress-range histograms are generated continuously and do not operate on triggers, thus all cycles are counted. Stress-range bins are divided into 0.5 ksi intervals and stress cycles less than 0.25 ksi were ignored. The stress-range bins are updated every 10 minutes to ensure that, in the event of a power failure, a minimum amount of data (*i.e., no more than 10 minutes worth*) would be lost.

3.2.3 Triggered Time Histories

During the long-term monitoring period, time history data are recorded when the wind speed exceeded predetermined levels or “triggers”. Once the predetermined wind speed levels were exceeded, time history data are recorded.

Separate triggers and data files are written for different wind speed thresholds. This was done to ensure that the memory card in the data logger would not fill up with low speed wind data in the event of a long wind event. For example, assume a major wind event was forecast for the Philadelphia region for a period of 24 hours. Further assume that during this event, winds are expected to be in excess of 35 mph for a significant amount of time with gusts reaching 60 mph. Obviously, prior to mean wind speeds reaching 35 mph, the mean wind speed had to increase from 10 through 30 mph. If the trigger threshold was set to say, 20 mph, the memory card could easily fill prior to the wind speed reaching mean wind speeds of 30 mph and the forecast peak gusts. In order to ensure that memory is available, predefined data tables are set up in the program. Trigger levels of 20, 30, 40, 50, and 60 mph were used. (*It should be noted that the 20 mph table has been removed since a sufficient amount of data have been collected for this range of wind speeds. The remaining memory has been allocated to the other tables.*)

In order to capture the entire event, data were recorded prior to the trigger event for a specified interval. For example, data were recorded for 60 seconds prior to the wind speed reaching the predefined trigger, (i.e., an 60 second buffer was maintained). The data acquisition system recorded for 90 additional seconds and then stopped only if the triggers were no longer satisfied. Thus, the minimum file length in this case would be 150 seconds (*60 + 90 = 150*).

The appropriate intervals for the pre- and post-triggers and the trigger thresholds were based on previous experience with monitoring similar structures and the controlled load data. Pre- and post-trigger recording times are not the same for all wind speed tables. Longer pre- and post-trigger intervals are specified for the higher wind-speed triggered events in order to more fully capture the event.

3.3 Destructive Testing

A destructive laboratory investigation of a total of ten cantilevered signal-support structures received from the City of Philadelphia was conducted. These poles were removed from service after having been in use for a number of years. The connections were selectively cut apart. The weldments were polished and etched and subsequently examined for the presence of fatigue cracks or defects. Complete details and findings of this investigation are contained in Appendix B.

4.0 Results of Controlled Load Tests

The results of the static and dynamic controlled load tests are discussed in this section. The results for each pole will be presented separately and then compared.

4.1 84th and Lindbergh

4.1.1 Static Tests – Vertical Loading

Vertical loads were applied at the tip of the mast-arm as described in Section 3.1. The results of the measurements are summarized in Table 4.1. Figure 4.1 presents measured stresses at gages at the bottom of the column as a 100 lb load was applied. Although the load was applied statically, it was relatively windy while the tests were being conducted. As a result, small stress cycles were observed in the data. In addition, occasional "noise" spikes were observed in the data when the signals would change from green, to orange, to red. These are indicated in Figure 4.1 and were typical for most tests.

Channel	Load Case		Channel	Load Case	
	Vertical (ksi)	Horizontal (ksi)		Vertical (ksi)	Horizontal (ksi)
CH_1	0.0	0.1	**CH_9**	-2.3	0.1
CH_2	0.6	0.0	**CH_10**	-0.2	-3.5
CH_3	0.1	0.6	**CH_11**	1.6	-2.2
CH_4	-0.6	0.0	**CH_12**	BAD	BAD
CH_5	1.2	1.3	**CH_13**	0.2	0.0
CH_6	1.6	-0.7	**CH_14**	-0.4	0.6
CH_7	2.6	-0.3	**CH_15**	0.5	-5.5
CH_8	-0.2	3.0	**Displ. (inch)**	-4.4	Note 1

Notes

1. Displacement sensor not connected.

Table 4.1 – Summary of static stresses measured at structure located at 84th and Lindbergh.

Channels CH_2 and CH_4 are located on the rear (tension) and front (compression) sides of the pole respectively. As expected, nearly equal and opposite stresses are measured at channels CH_2 and CH_4. However, note the response at channel CH_5 and CH_6, which are located "in-line" with the anchor rods at the rear of the base plate. The stress in these bolts is between 2 to 3 times greater than measured at channel CH_2. The increase in stress near the bolts is primarily the result of flexibility (bending) of the base plate and shear lag. Behavior such as this has been observed in other similar structures.

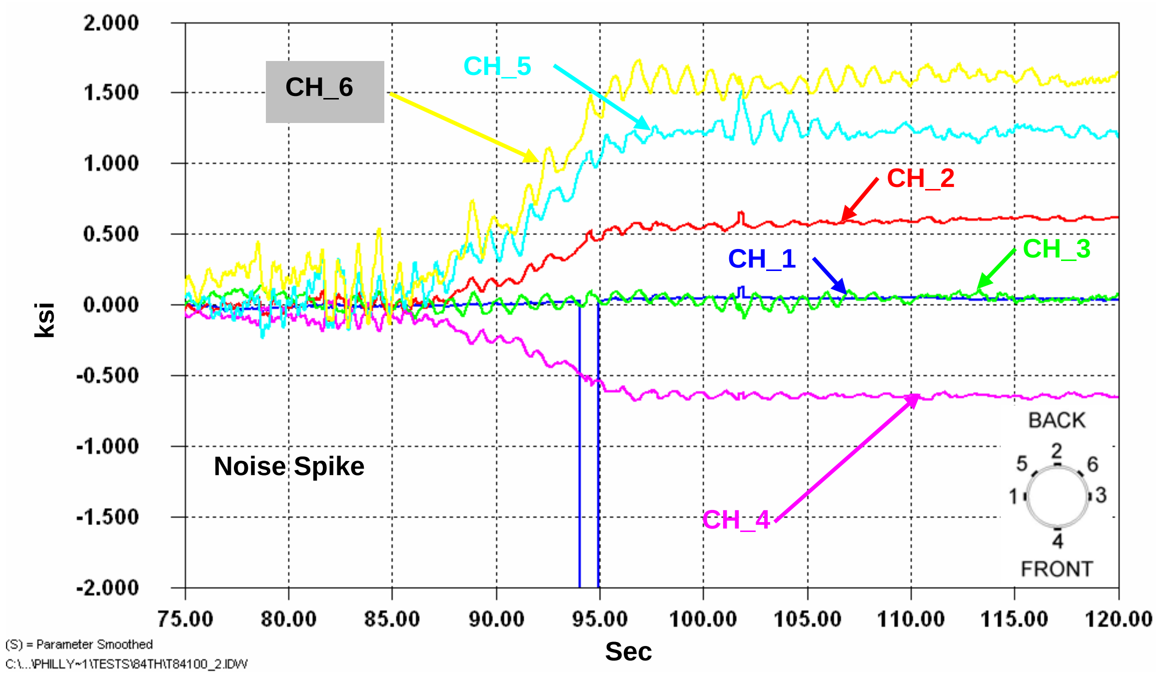

Figure 4.1 - Stresses at base of pole as 100 lb load is applied at tip of mast-arm (84th and Lindbergh)

Although the base plate is mounted on grout, the tension portion of the bending moment couple in the tube must be resisted entirely by the rear anchor rods. Basic mechanics of materials calculations indicate the greatest stress is at the rear of the pole between the anchor rods (*i.e., at the position of channel CH_2*). In reality, the base plate is very flexible between the bolts. As a result, little load can be transferred from the back of the pole to the bolts. Hence, the rear portion of the tube between the anchor rods is not as effective in transferring the bending moment in the area adjacent to the base plate as assumed. *(Current design practice assumes the base plate is infinitely rigid)* As a result, stresses are greater near the anchor rods, where most of the moment is resisted.

As discussed, gages were also installed on the mast-arm adjacent to the upper flange plate connection. Gages were installed in a similar pattern around the mast-arm (See Figure 2.1). Figure 4.2 presents the response from these gages as the 100 lb load was suspended from the tip of the mast-arm. Channel CH_12 was not working during this test.

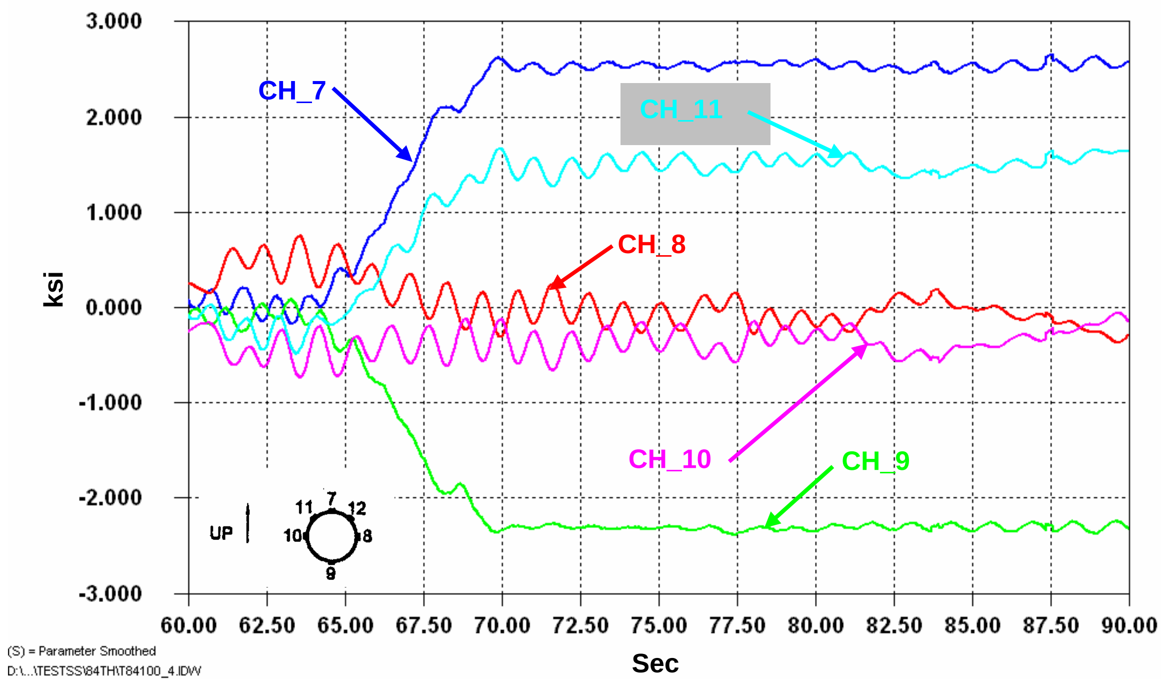

Figure 4.2 - Stresses in mast-arm adjacent to flange plate connection to pole as 100 lb load is applied at tip of mast-arm (84th and Lindbergh)

As can be seen stresses in channels CH_7 and CH_9 are nearly equal and opposite, with slightly greater stress measured at channel CH_7. Very little stress is measured at channels CH_8 and CH_10, located at the theoretical neutral axis. The small variations in stress, primarily observed in channels CH_8 and CH_10 are the result of wind blowing on the mast-arm during the test. Nevertheless, a slight decrease in the mean stress of channels CH_8 and CH_10 is apparent in Figure 4.2 as the load is applied. A similar trend was observed in all four tests in which the 100 lb load was suspended from the tip of the mast-arm at this pole. The slight offset suggests that the actual neutral axis is slightly below the theoretical neutral axis. This observation is in agreement with the measurements at channel CH_7 and CH_9, which suggest the neutral axis is about 0.25 inches below the theoretical neutral axis.

It should be noted that the stress measured at channel CH_11 is less than that at channel CH_7. This behavior is not consistent with the measurements made at the base plate detail (See Figure 4.1). The flange plate at the mast-arm connection is stiffer than the base plate. There are three primary reasons for the increase in stiffness at the upper connection. First, the flange plate on the mast-arm is slightly thicker than the base plate (*1.25 inches vs. 1.00 inch*). Second, the flange plate of the mast-arm is bolted to the flange plate on the pole. Since the four bolts have some level of pretension, the two plates act together to a certain degree, effectively increasing the stiffness of the plate. Third, the bolts are more closely spaced at the top flange plates. In the base plate, the anchor rods are spaced at 13 inches. In the flange plate of the mast-arm the bolts are spaced at 11.5 inches. All three of these factors combine to increase the effective stiffness of the flange plate resulting in a more uniform distribution of stress in the mast-arm at the connection.

4.1.2 Static Tests – Horizontal Loading

Horizontal load was also applied at tip of the mast-arm. However, during the tests, natural wind gusts were rather high. Wind primarily applies horizontal loading to the pole and introduces similar stresses as the horizontal loads applied during the controlled tests. As a result, the data collected during these tests contains cyclic stresses induced by natural wind.

Similar to the tests conducted with vertical loads applied, channels CH_5 and CH_6 were subjected to the greatest stress range, as shown in Figure 4.3. The stresses measured at channel CH_5 and CH_6 were compression and tension respectively. The data were also consistent with the direction of applied loading. Interestingly, the stresses at gages CH_5 and CH_6 were higher than at channel CH_1 and CH_3, located on the primary axis for the reasons discussed above. It is interesting to note that the stress at channel CH_3, on the tension side, was considerably greater than measured at channel CH_1. (*As will be discussed, a similar observation was noted at the pole at Island Avenue*.) The exact reason for this behavior is not clear.

It should be noted that the cyclic stresses observed at channels CH_5 and CH_6 are due to vertical motion of the mast-arm. Figure 4.4 is a detail of data between time equal to 65 and 70 seconds shown in Figure 4.3. The data demonstrate that the cycles at CH_5 and CH_6 are in phase. Also shown are the measurements from channels CH_2 and CH_4, which are out-of-phase. Hence, the movement is in the vertical plane of the mast-arm.

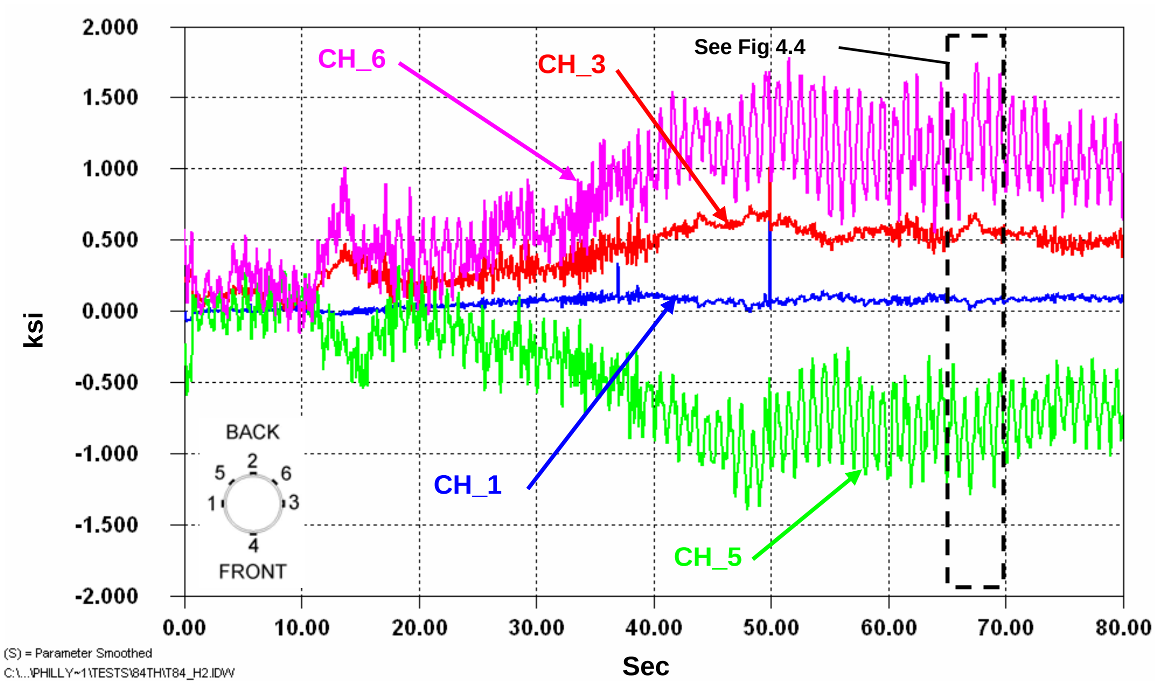

Figure 4.3 - Stresses at base of pole as horizontal force is applied at tip of mast-arm (84th and Lindbergh)

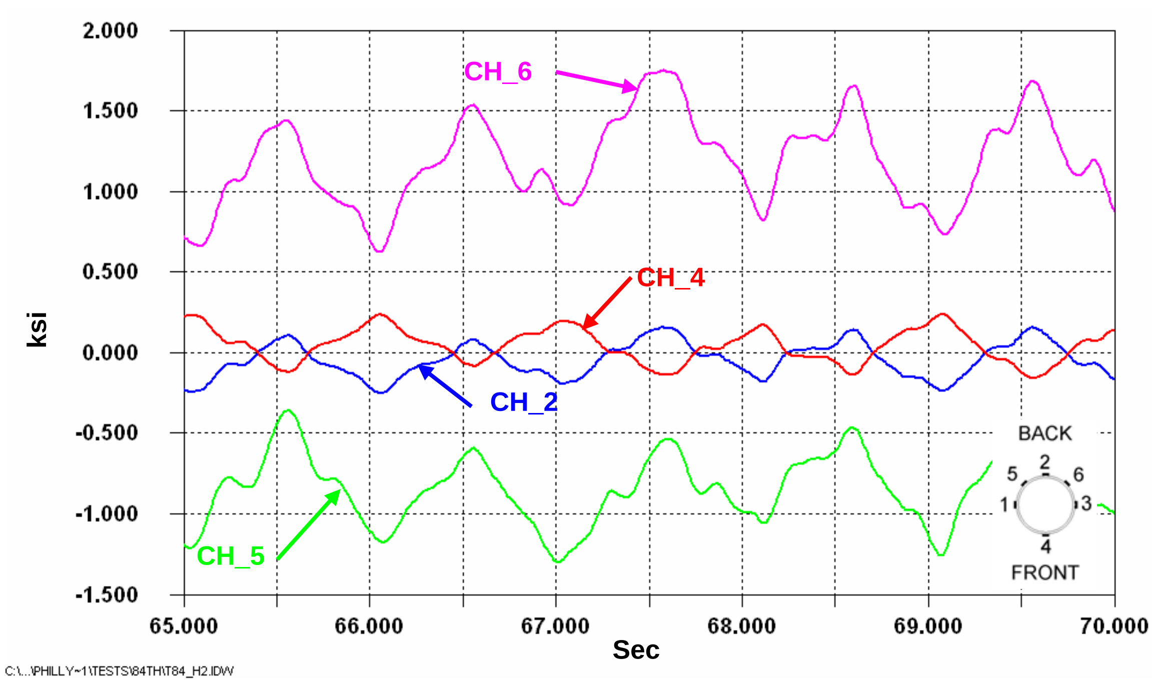

Figure 4.4 - Detail of stresses at base of pole as horizontal force is applied at tip of mast-arm. Note response of channels CH_5 and CH_6 and CH_2 and CH_4 indicating vertical hatcheting movement of pole (84th and Lindbergh))

4.2 Island Avenue and SR 291

4.2.1 Static Tests – Vertical Loading

A series of static tests were conducted on the pole located at Island Avenue and SR 291. The structure is similar to the one located at 84th and Lindbergh. The instrumentation installed on the mast-arm and pole was identical. However, strain gages were not installed on the plates that attach the flange plate to the pole. The results of all tests are summarized in Table 4.2.

Channel	Load Case		Channel	Load Case	
	Vertical (ksi)	Horizontal (ksi)		Vertical (ksi)	Horizontal (ksi)
CH_1	0.0	0.2	**CH_8**	-3.1	3.5
CH_2	0.5	-0.2	**CH_9**	0.0	0.1
CH_3	0.0	0.0	**CH_10**	-3.0	-3.6
CH_4	-0.6	-0.2	**CH_11**	2.0	-1.4
CH_5	1.5	-0.7	**CH_12**	3.4	2.7
CH_6	1.8	0.9	**Displ. (inch)**	-5.6	Note 1
CH_7	3.0	-0.3	**-**	**-**	**-**

Notes

1. Displacement sensor not connected.

Table 4.2 – Summary of static stresses measured at structure located at Island Ave. and SR 291.

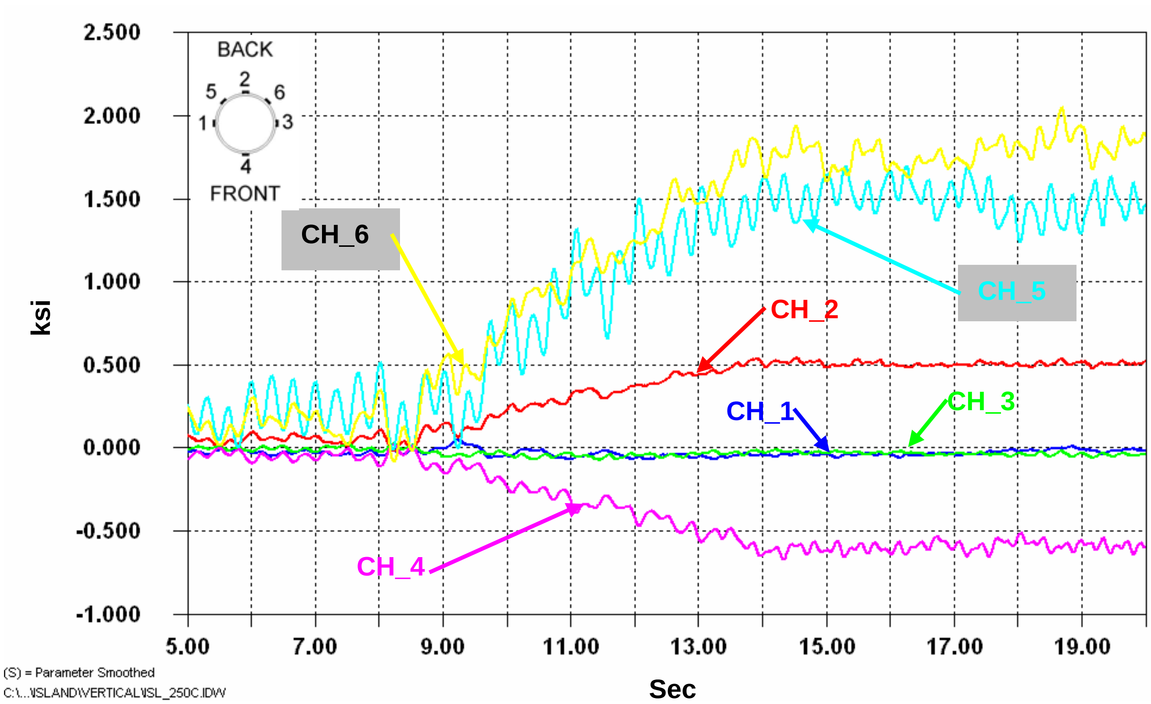

Figure 4.5 - Detail of stresses at base of pole as vertical force is applied at tip of mast-arm. (Island Ave. and SR 291))

Figure 4.5 presents the response of the pole adjacent to the base plate as a vertical load of 100 lbs was applied at the tip of the mast-arm. Comparing the results to the response with the pole at 84th street in Figure 4.1 shows nearly identical results. The most important observation is again related to the higher than expected stresses at channels CH_5 and CH_6. The reason for the higher than anticipated stresses at CH_5 and CH_6 was previously discussed.

Figure 4.6 presents the response in the <u>mast-arm</u> as the 100 lb load was applied. The response is considerably different than expected and observed in the mast-arm at 84th street. Channel CH_9 indicates nearly no compressive stress is carried through the bottom portion of the mast-arm. However, channels CH_8 and CH_10, which are located at the theoretical neutral axis (*for vertical bending*), show that the mast-arm is subjected to a significant compression stress at the mid-depth. All instrumentation was closely checked to verify that the measured behavior was not due to mis-wiring or some other problem. It was found that all instrumentation was working properly and that the measured stresses were correct.

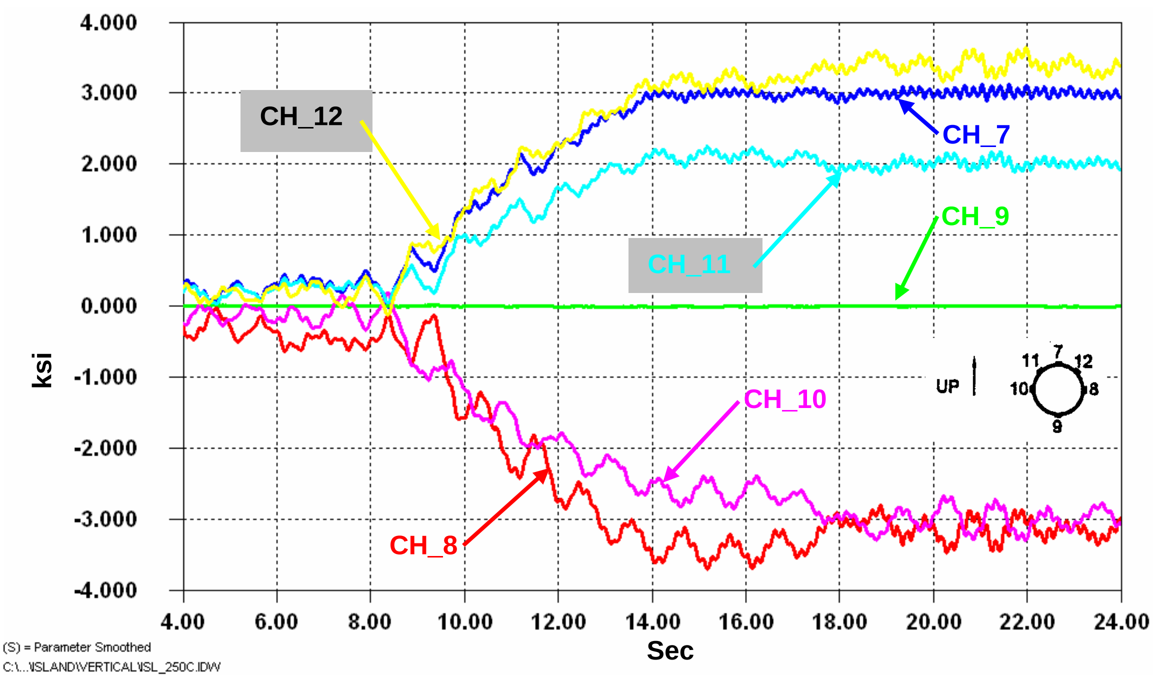

Figure 4.6 - Stresses in mast-arm adjacent to flange plate connection to pole as 100 lb vertical load is applied at tip of mast-arm (Island Ave. and SR 291)

In order to establish the cause of the observed behavior, a close-up inspection was made of the upper mast-arm flange connection. The inspection revealed that the flange plates were not in full contact, especially at the lower portion of the connection. Figure 4.7 is a photograph of this detail and clearly shows the gap between the flange plates. Although all four bolts appear to be tight, the preload was apparently insufficient to close the gap.

It is clear from the photograph that there is no contact between the flange plates at the elevation where the bottom portion of the mast-arm tube is welded to the flange plate. Hence, there is no path for compression stresses in the bottom of the tube to follow into the flange plate.

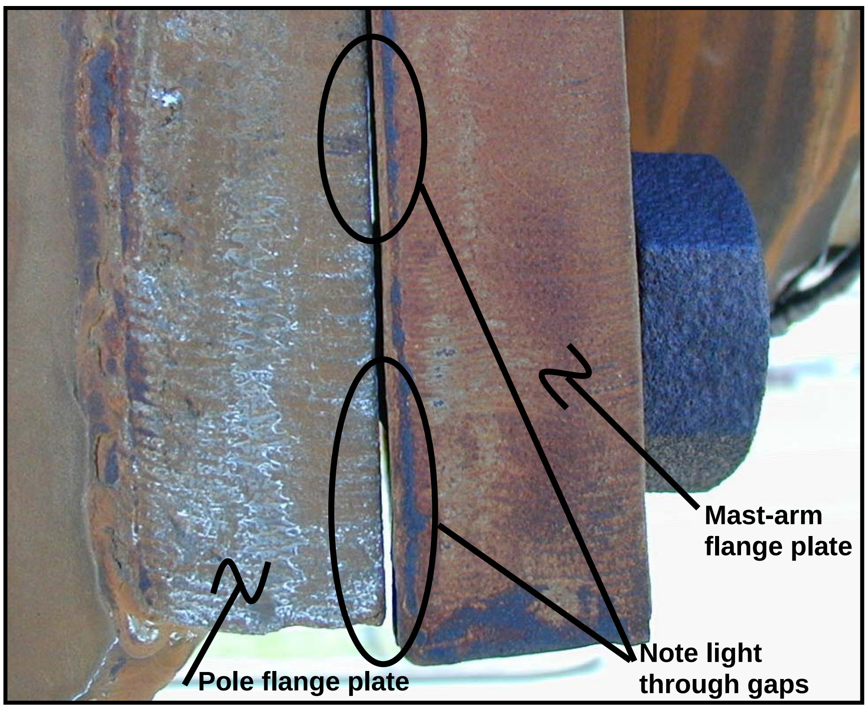

Figure 4.7 - Photograph of flange plate connection showing gap between plates
(Island Avenue and SR 291)

The behavior is presented schematically in Figure 4.8 and illustrates why little to no stress was measured at channel CH_9. Because of the gap at the Island Avenue pole, the bending moment must be resisted by a reduced section of the mast-arm near the flange plate. Hence, the neutral axis shifts upward, as shown in Figure 4.8 and gages at the mid-depth of the mast-arm (i.e., CH_8 and CH_10) are subjected to compression stresses.

Clearly, gaps, such as the one shown in Figure 4.8 can significantly alter the stress field in the region of the connection. As a result, traditional mechanics of materials calculations will under predict the stress range in the mast-arm and the bolts in the flange plates.

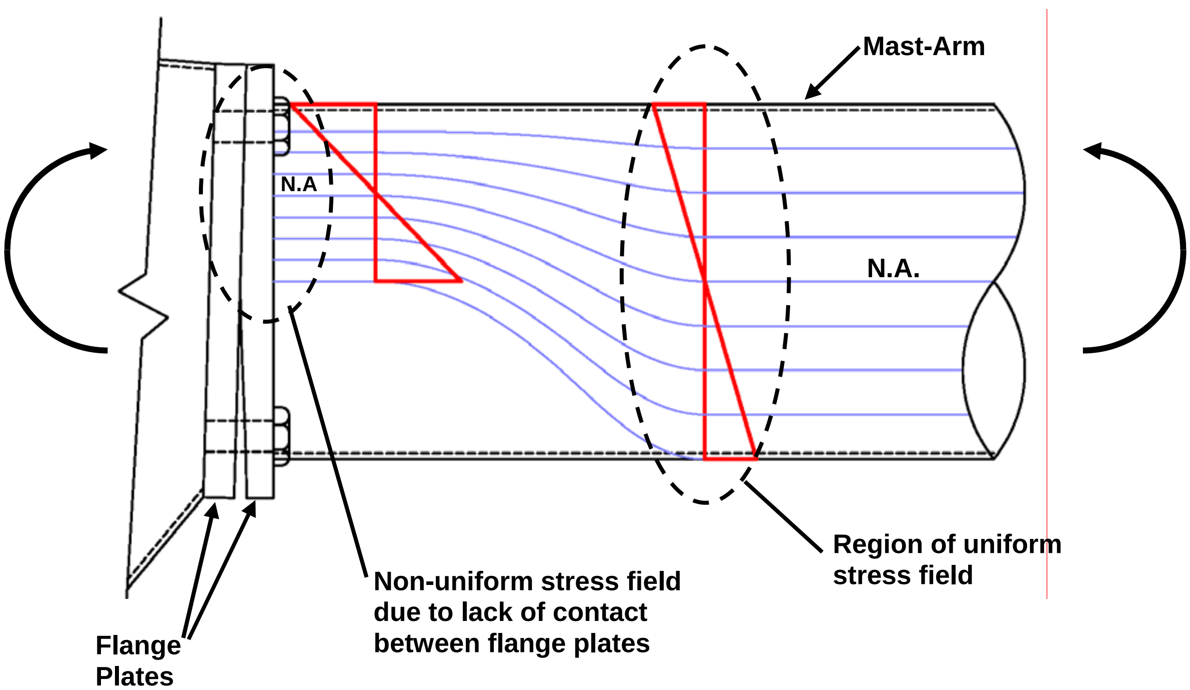

Figure 4.8 - Illustration of stress field in mast-arm due to lack of bearing between flange plates

4.2.2 Static Tests – Horizontal Loading

Horizontal load was applied at the tip of the mast-arm by attaching a wire to the man basket and slowly moving the man basket away from the mast-arm. Care was taken to ensure that the load was applied in the horizontal plane as much as possible. The magnitude of the load could not be measured for these tests. However, the results provide insight into the behavior of the structure when subjected to horizontal loading. Results of all tests are summarized in Table 4.2.

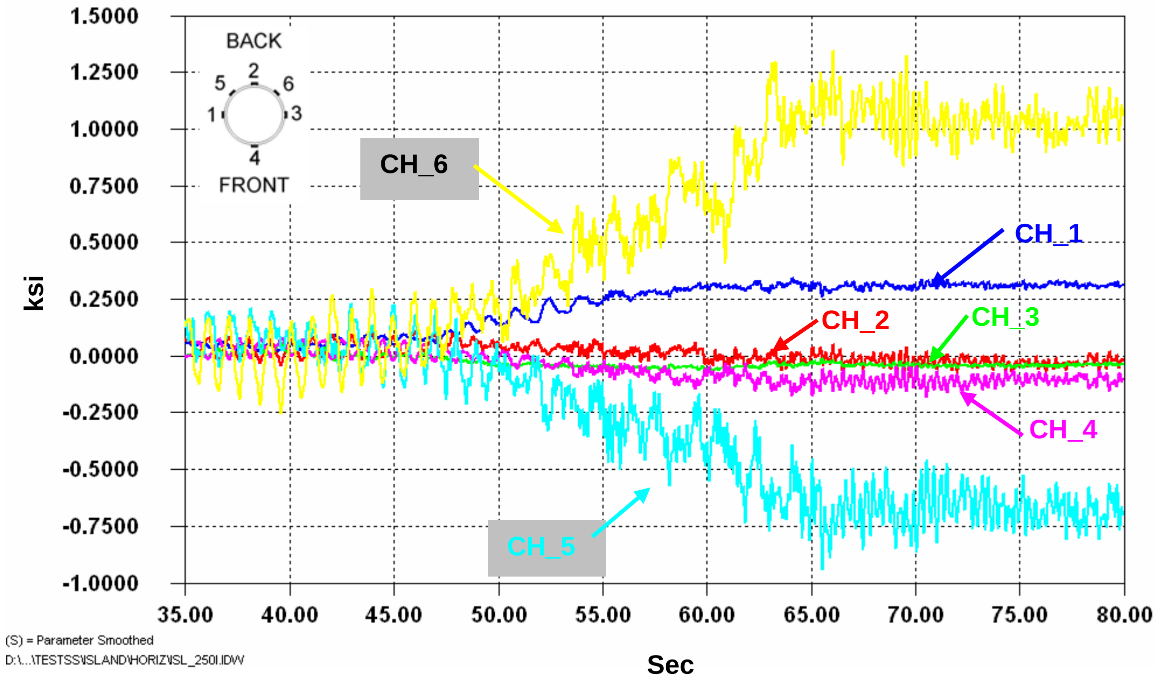

Figure 4.9 - Stresses in mast-arm at base of pole as horizontal load is applied at tip of mast-arm (Island Ave. and SR 291)

Figure 4.9 presents the response at the base of the pole as horizontal load was applied at the tip of the mast-arm. The response of the pole is essentially the same as what was observed in the pole at 84th street. *(The magnitude of the stresses at 84th Street are different since different loads were applied. However, the overall behavior is in very good agreement.)* Interestingly, channel CH_1, on the tension side of the pole, exhibits a much greater proportion of stress than channel CH_3 on the compression side. Theoretically, the response at CH_1 and CH_3 should be equal and opposite. However, this is not the case as demonstrated in Figure 4.9. Recall, the same type of response was observed in the pole at 84th street as horizontal load was applied. The exact cause for this behavior is unknown.

Figure 4.10 presents the response of the mast-arm subjected to the same load in Figure 4.9. As expected, channel CH_8 and CH_10 are exhibit the greatest stress and are approximately equal and opposite in sign. The response at CH_7 and CH_9 are nearly zero, as expected. Recall that the lower portion of the mast-arm flange plate was not in contact with the flange plate on the pole and a gap was observed (See Figure 4.7). Channels CH_11 and CH_12 would be expected to be subjected to equal and opposite stresses. However, the measurements indicated otherwise. This may be the result of the gap at the lower portion of the flange plates or some other effect, such as a loose bolt.

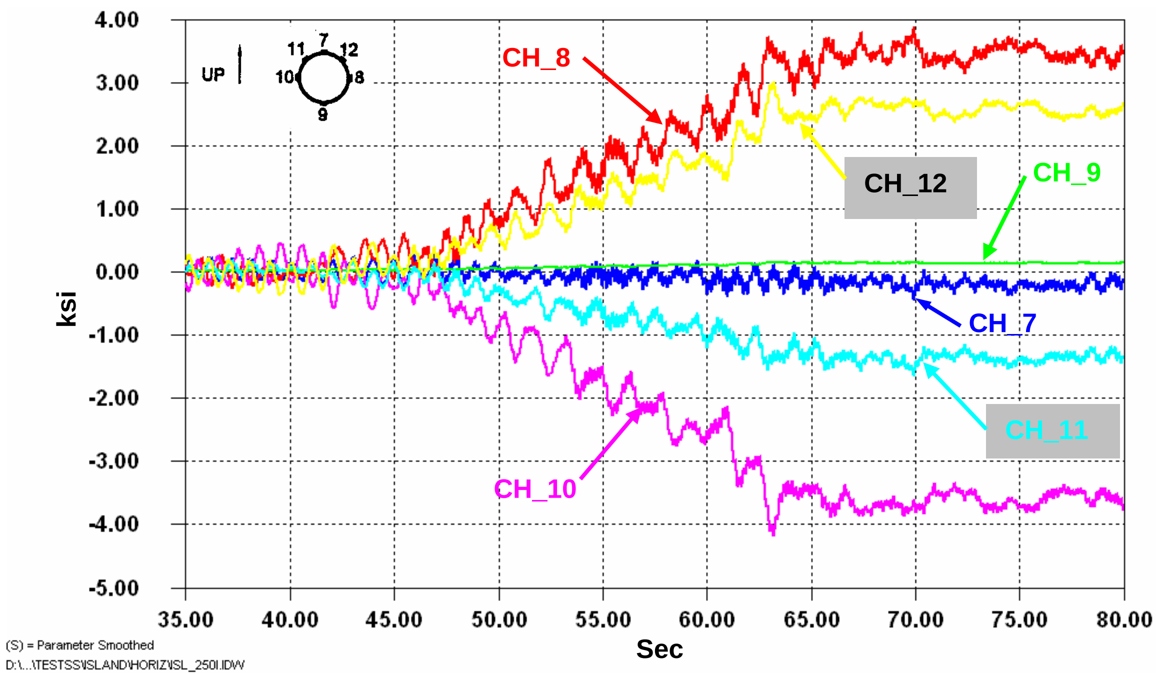

Figure 4.10 - Stresses in mast-arm adjacent to flange plate connection to pole as horizontal load is applied to tip of mast-arm (Island Ave. and SR 291)

4.3 Summary of Controlled Load Tests

The results of the controlled load tests have been discussed. The following observations and concludes are made:

- Both poles behave similarly under vertical and horizontal static loads.
- Base plate flexibility greatly alters the stress distribution in the wall of pole and base plate. Higher than expected stresses were measured in the pole nearer the anchor rods.
- Base plate flexibility results in bending of the base plate and additional bending of the anchor rods. Increased bending of the anchor rods can result in decrease fatigue life.
- Lack of full contact between flange plates (Island Ave) and/or loose bolts significantly alters the stress distribution in the mast-arm near the connection.
- Lack of full contact between the flange plates increases the stress range in the bolts used to connect the flange plate.

5.0 Results of Dynamic Load Tests

The results of the dynamic field tests for both cantilevered mast-arm structures are discussed in this section. Both controlled and uncontrolled dynamic tests were performed. The results for each pole will be presented separately and then compared.

As discussed previously, vertical and horizontal static load tests were conducted. Vertical static load was applied with a 100 lb weight hung from the cantilever tip. Horizontal static load was applied using the manlift. In order to investigate the dynamic characteristics of the poles, the static load was removed from the pole suddenly by cutting the wire to which the load was attached. This sudden release of load put the pole into free vibration. Strain, displacement, and acceleration data were recorded at a high sampling rate to ensure that all critical dynamic behavior is captured.

During free vibration, several modes of vibration were observed which will be discussed. The attenuation of the vibration can be quantified through the use of the damping ratio which was calculated. The rate of attenuation can have a major effect on the number of stress cycles to which the structure is subjected. Finally, the use of acceleration data to determine the displacement time history (by double integration) is evaluated by comparing calculated values to directly measured displacements.

As indicated above, each test was performed multiple times. Examination of the data reveals that the for multiple tests, the data are repeatable and consistent. Therefore, only one data set for each test is used for data reduction and analysis.

Data were recorded while the cantilevered mast-arms were subjected to ambient vibration caused by wind loading. These data will also be presented and discussed.

5.1 84th and Lindbergh

5.1.1 Free Vibration Tests – General Response

A typical stress time-history of CH_5 during vertical free vibration of the pole is contained in Figure 5.1. The plot shows nearly one minute of data after the load is released. It is interesting to note that the vibration appears to be dominated by first mode response. Furthermore, the amplitude of vibration attenuates very slowly, which indicates a low level of damping in the structure for this vertical mode of vibration.

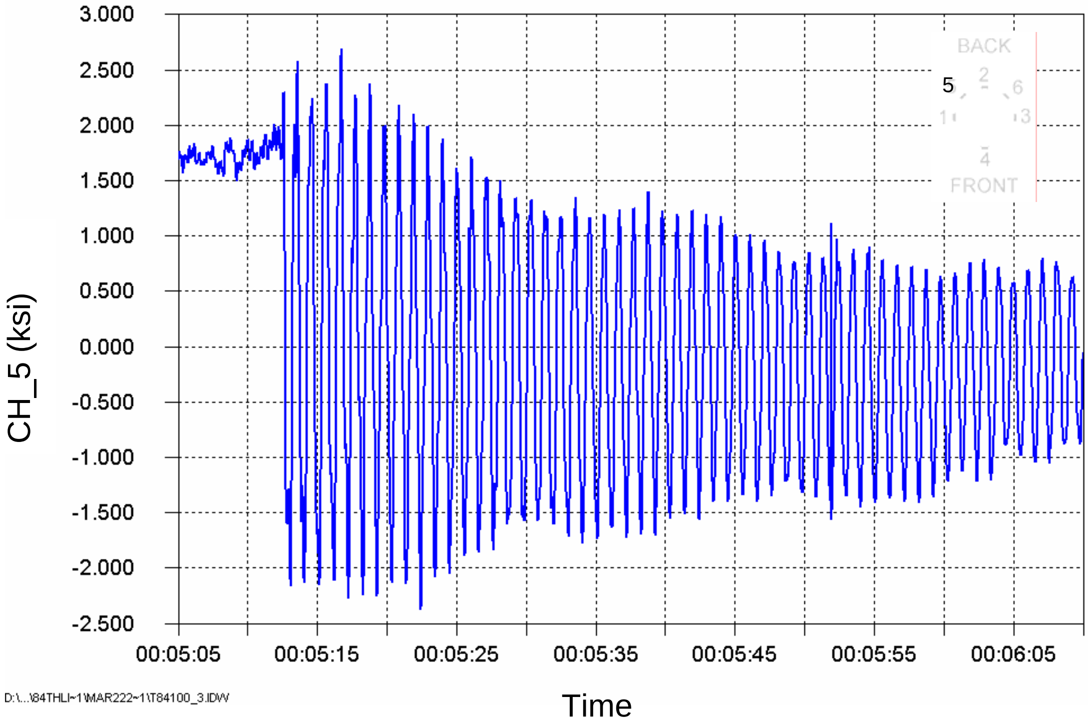

Figure 5.1 - Stresses at strain gage CH_5 as 100 lb vertical load is released from tip of mast-arm (84th and Lindbergh)

Figure 5.2 contains a similar stress time-history of strain gage CH_8 during horizontal free vibration of the mast-arm. As shown, this plot contains about 30 seconds of free vibration response. The free vibration for this horizontal mode damps out much more rapidly than the vertical mode. However, similar to the vertical vibration test, the response appears to be dominated by first mode response.

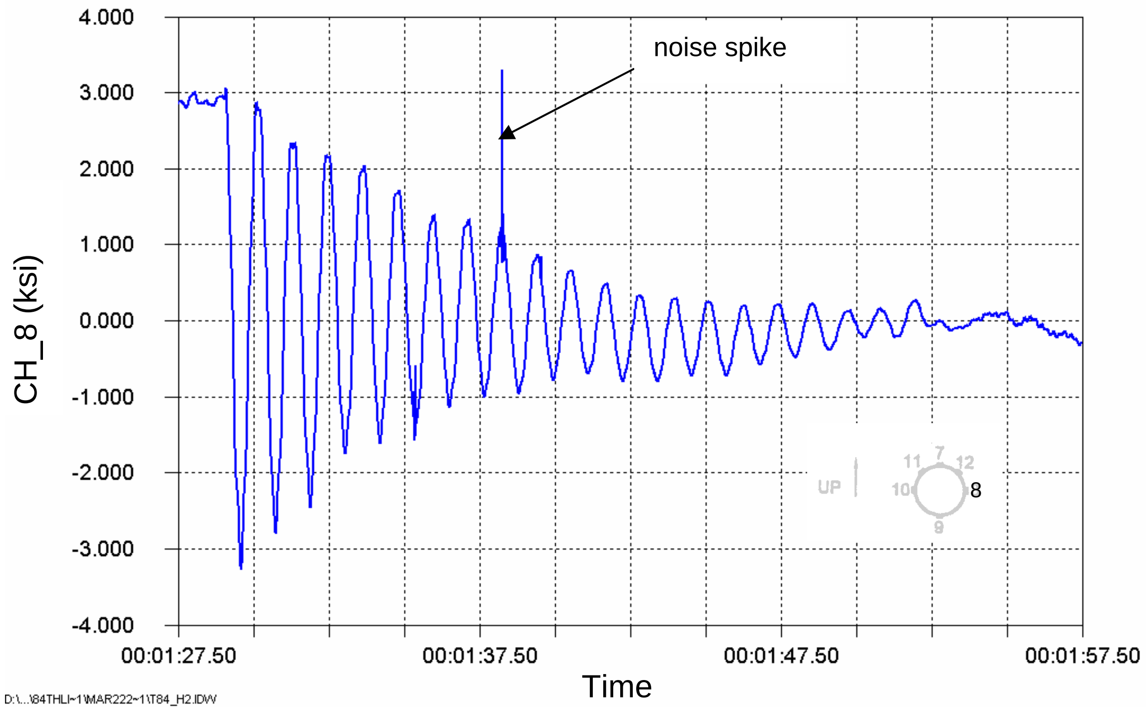

Figure 5.2 - Stresses at strain gage CH_8 as horizontal load is released from tip of mast-arm (84th and Lindbergh)

5.1.2 Mode Shapes

The cantilever mast-arms structures appear to have two primary modes of vibration, with additional harmonic modes of each. The first mode, observed in the vertical free vibration load tests, is called the "hatcheting" mode. The next mode, observed in the horizontal free vibration tests, is called the "torsional" mode. These mode shapes are illustrated in Figure 5.3.

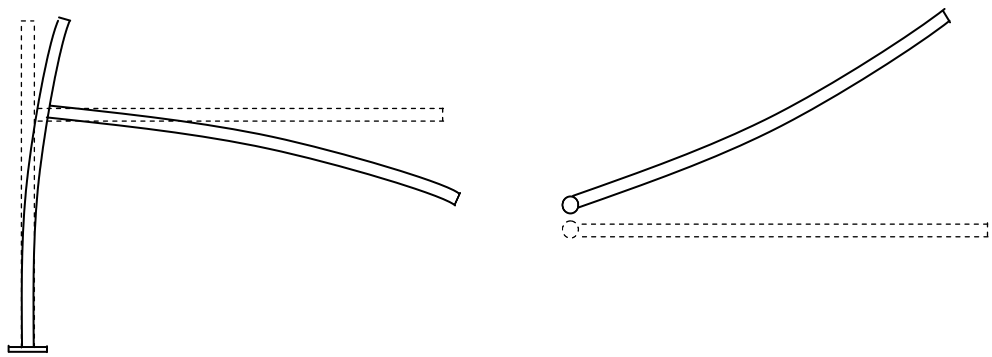

(a) "Hatcheting" Mode -Elevation View (b) "Torsional" Mode - Plan View

Figure 5.3 – Two primary modes of vibration: (a) "hatcheting" mode, and (b) "torsional" mode

5.1.3 Modal Frequencies

The frequency spectra for each test are obtained by performing Fast Fourier Transforms (FFT) on the free vibration portion of the time-history data. The acceleration time-history data is used since higher modes of vibration are not evident in the strain gage data.

The frequency spectrum provides an estimate of the fundamental frequencies of vibration of the structure. Figure 5.4 contains the frequency spectrum of the vertical acceleration time-history. The three peaks represent the first three hatcheting modes of vibration, and have frequencies of 0.95 Hz, 2.91 Hz, and 5.35 Hz.

Figure 5.5 contains the frequency spectrum of the horizontal acceleration time-history. The three peaks represent the first three torsional modes of vibration, and have frequencies of 0.88 Hz, 3.12 Hz, and 5.22 Hz.

It can be seen that the harmonics of the torsional and hatcheting modes are closely spaced. For example, the frequency of the 2nd hatcheting mode (2.91 Hz) is very close to the 2nd torsional mode (3.12 Hz).

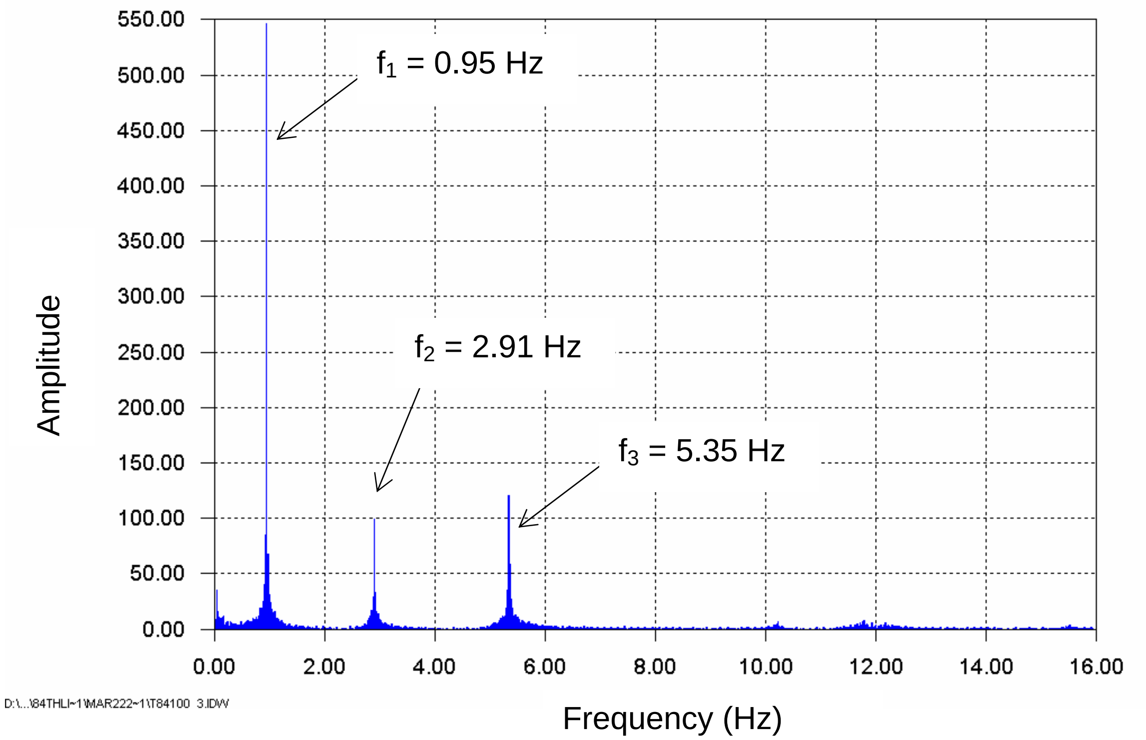

Figure 5.4 – Frequency spectrum of vertical acceleration at the tip of the mast-arm during vertical free vibration test (84th and Lindbergh)

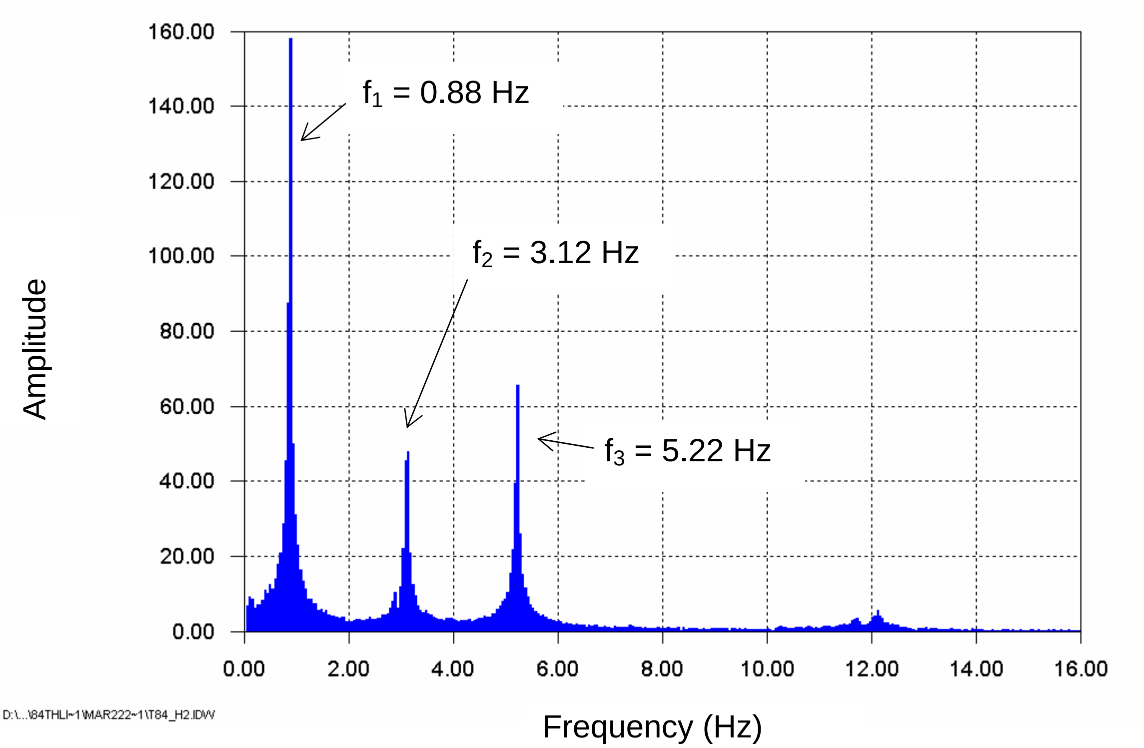

Figure 5.5 – Frequency spectrum of horizontal acceleration at the tip of the mast-arm during horizontal free vibration test (84th and Lindbergh)

5.1.4 Damping Ratios

As noted previously, these mast-arm structures have different damping characteristics for hatcheting and torsional motion. The structural damping can be estimated from the time-history data using the logarithmic decrement method. Given the values of the response at two peaks, and the number of cycles between those peaks, this method provides an estimate of the percent critical damping.

Using this method, the structural damping coefficient, ξ, is estimated to be 0.9% for the first hatcheting mode, and 2.5% for the first torsional mode. When the structure is vibrating in the hatcheting mode, it is clear that there is very low damping. Typical damping ratios for a steel structure are around 2-3%.

Under hatcheting vibration, there are few attachments or bolted connections where energy can be dissipated. However, when the mast-arm is under torsional vibration, the sleeve connections may slightly slip within each other. This friction provides for energy dissipation, and therefore raises the damping ratio for this mode of vibration.

5.1.5 Comparison of Measured and Calculated Displacement

Displacement of the tip of the mast-arm can be determined using acceleration data, by integrating the data twice, in conjunction with high-pass filtering to remove unwanted drift in the calculated results. As indicated previously, for certain tests, a displacement transducer was connected to the tip of the mast-arm. This data can be compared to the calculated displacements (using acceleration data) to demonstrate the validity of the results. It should be noted that during the monitoring phase of the project, the displacement transducer is not present. Therefore, the only way to determine displacements is to use acceleration data, and it is necessary to verify the calculated displacements.

Figure 5.6 contains a plot of a segment of measured and calculated displacements versus time, for a vertical free-vibration test. It can be seen that there is good agreement. Therefore, it is deemed acceptable to use acceleration data to determine displacements of the mast-arm during long-term monitoring.

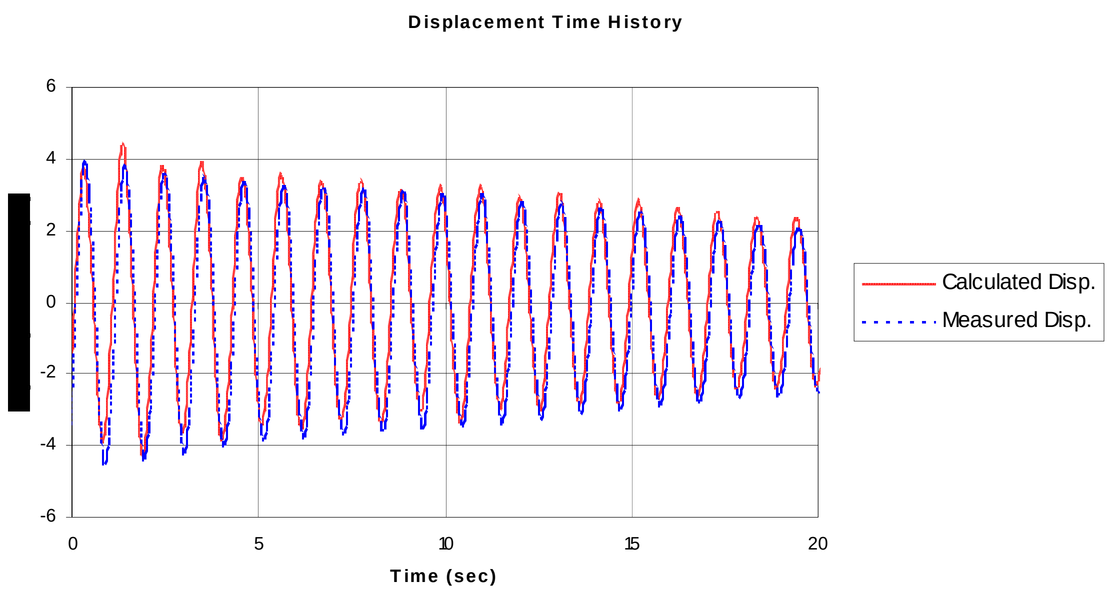

Figure 5.6 – Calculated and measured displacement versus time
for vertical free-vibration test (84th and Lindbergh)

5.1.6 Analysis of Ambient Vibration

Subsequent to performing controlled load tests on the mast-arm cantilever structure, uncontrolled tests were performed. Data were collected as the pole vibrated while subjected to ambient wind. An analysis of these data provides an understanding of the in-situ behavior of the pole.

Figure 5.7 contains a frequency spectrum of a 82 second block of data from strain gage CH_5, during ambient vibration. Recall that this gage is located near the column baseplate, directly adjacent to the anchor bolt. Since it is on the diagonal, this gage experiences stress due to both vertical and horizontal excitation (bending about either major axis of the column). The spectrum indicates three pairs of frequencies, as expected. These pairs represent the first, second, and third modes of vibration. Each pair is composed of a hatcheting and torsional mode of vibration. It can be seen that the frequencies in Figure 5.7 correspond well with the frequencies determined in the free vibration tests described above. It should be noted that the peak near zero frequency corresponds to an offset in the acceleration time-history data, and does not represent a real low frequency mode of vibration.

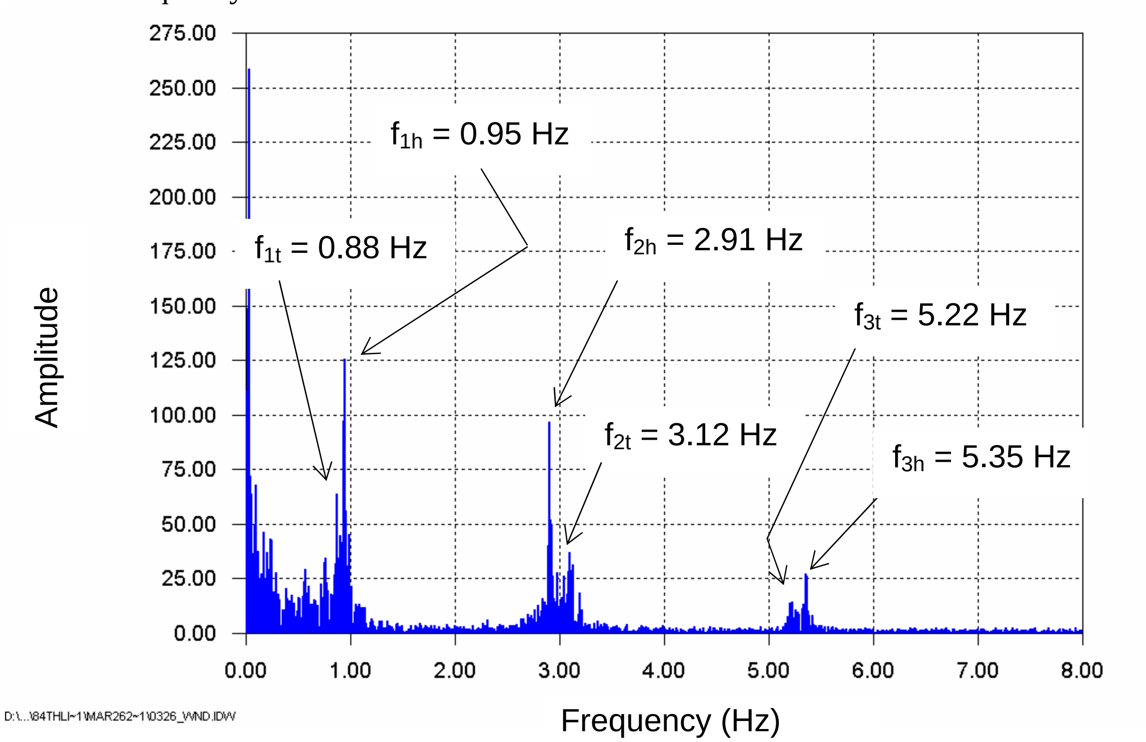

Figure 5.7 – Frequency spectrum for uncontrolled load tests of CH_5
(Note subscript "t" refers to torsional mode, "h" refers to hatcheting mode)
(84^{th} and Lindbergh)

5.2 Island Avenue and SR 291

5.2.1 Free Vibration Tests – General Response

The general dynamic response of the Island Avenue cantilevered mast-arm was similar to that of the Lindbergh/84th St. pole. However, there are some slight differences due to non-uniform bearing at the mast-arm-to-column flange connection discussed previously in Section 4, as well as minor differences in geometry and signal configuration.

A typical stress time-history of CH_5 during vertical free vibration of the pole is contained in Figure 5.8. The plot shows approximately 50 seconds of data after the load is released. It is interesting to note that unlike the Lindbergh site, the vibration appears to have several modes of vibration present in the strain data. Furthermore, the amplitude of the vibration attenuates more rapidly, which indicates a higher level of damping in this structure for the vertical mode of vibration.

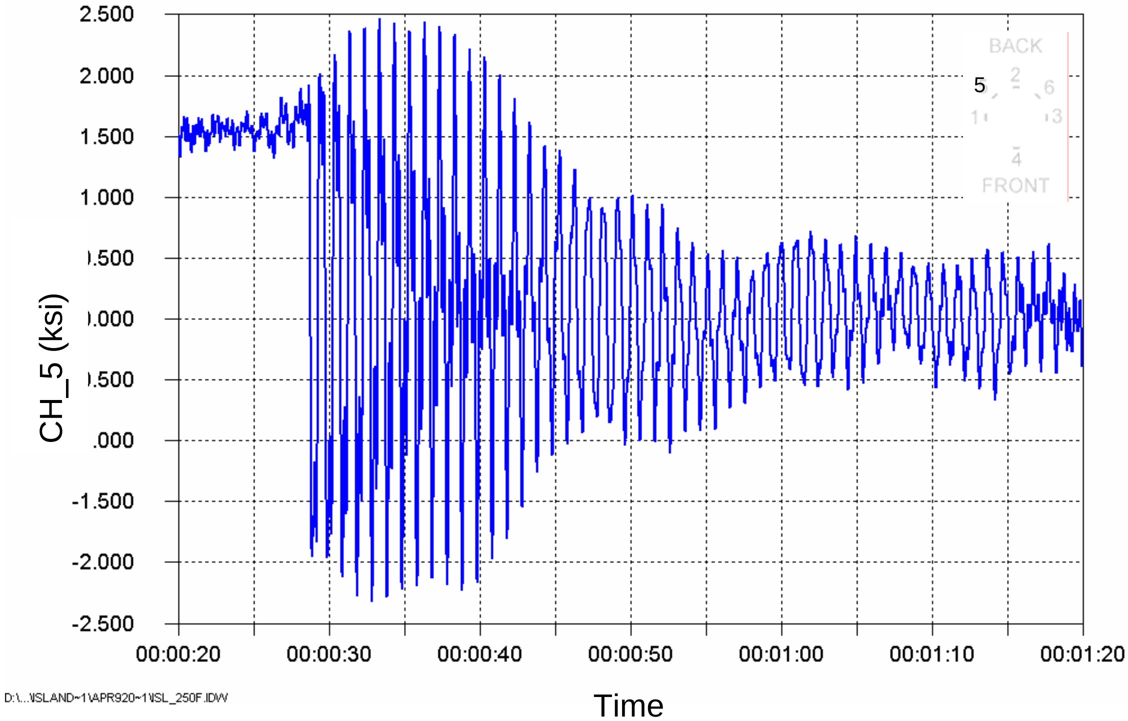

Figure 5.8 - Stresses at strain gage CH_5 as 100 lb vertical load is released from tip of mast-arm (Island and SR 291)

Figure 5.9 contains a similar stress time-history of strain gage CH_8 during horizontal free vibration of the mast-arm. As shown, this plot contains about 30 seconds of free vibration response. The free vibration for this horizontal mode damps out more quickly than the vertical mode. Unlike the vertical vibration test, the horizontal response appears to be dominated by the first mode.

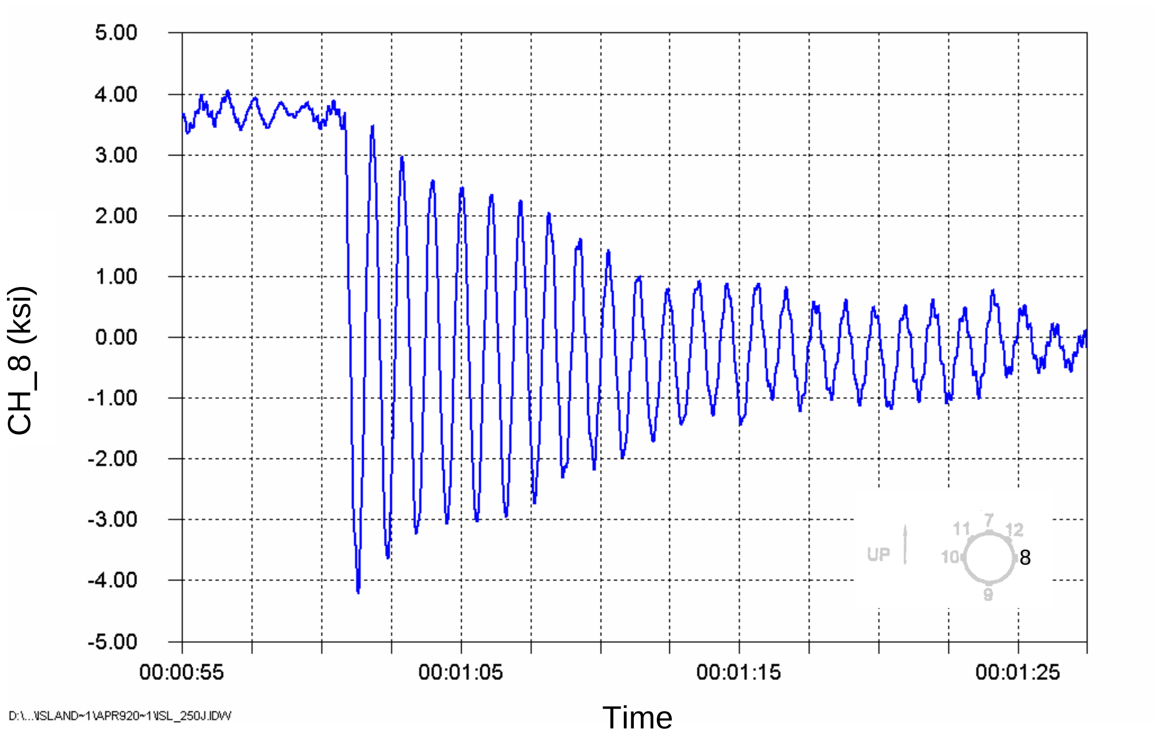

Figure 5.9 - Stresses at strain gage CH_8 as horizontal load is released from tip of mast-arm (Island and SR 291)

5.2.2 Mode Shapes

This cantilever mast-arm structure appears to have the same two primary modes of vibration (hatcheting and torsion) as discussed previously, and illustrated in Figure 5.3.

5.2.3 Modal Frequencies

The amplitude spectrum provides an estimate of the fundamental frequencies of vibration of the structure. Figure 5.10 contains the frequency spectrum of the vertical acceleration time-history. The three peaks represent the first three hatcheting modes of vibration, and have frequencies of 1.04 Hz, 2.99 Hz, and 5.00 Hz. These frequencies are very similar to those of the 84th and Lindbergh pole.

Figure 5.11 contains the frequency spectrum of the horizontal acceleration time-history. The three peaks represent the first three torsional modes of vibration, and have frequencies of 0.92 Hz, 3.05 Hz, and 5.37 Hz. Again, these values are very close to those of the 84th and Lindbergh pole. As before, it can be seen that the harmonics of the torsional and hatcheting modes are closely spaced.

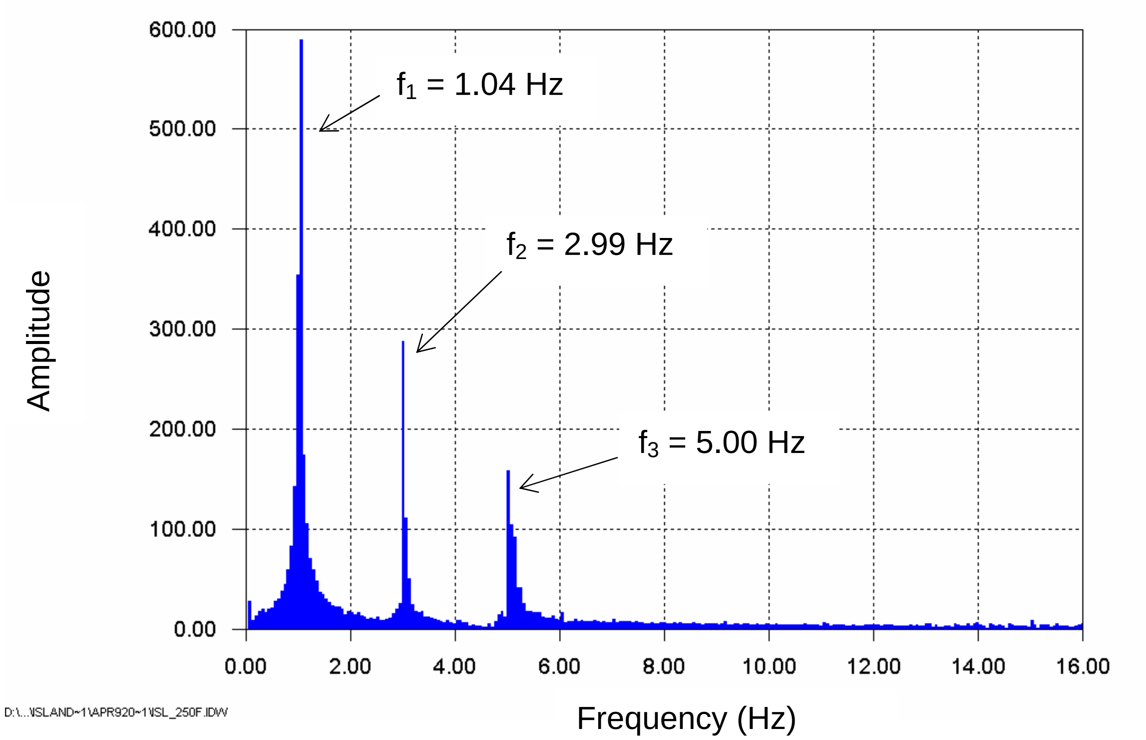

Figure 5.10 – Frequency spectrum of vertical acceleration at tip of mast-arm during vertical free vibration test (Island and SR 291)

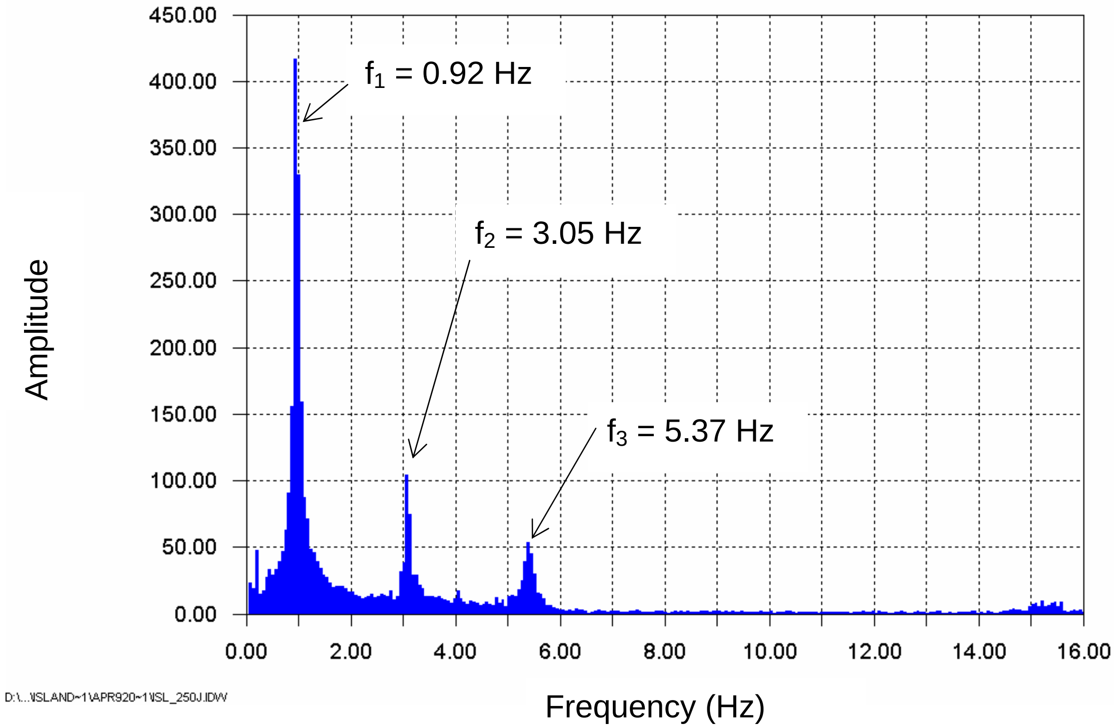

Figure 5.11 – Frequency spectrum of horizontal acceleration at tip of mast-arm during horizontal free vibration test (Island and SR 291)

5.2.4 Damping Ratios

The structural damping coefficient, ξ, for this pole is estimated to be 1.0% for the first hatcheting mode, and 1.4% for the first torsional mode. The damping for the vertical mode is similar to the other location, however, the damping for the horizontal mode is significantly less.

5.2.5 Analysis of Ambient Vibration

Figure 5.12 contains a frequency spectrum of a 82 second block of data from strain gage CH_5, during ambient vibration. Recall that this gage is located near the column baseplate, directly adjacent to the anchor bolt. Since it is on the diagonal, this gage experiences stress due to both vertical and horizontal excitation (bending about either axis of the column). The spectrum indicates three pairs of frequencies, as expected. These pairs represent the first, second, and third modes of vibration. Each pair is composed of a hatcheting and torsional mode of vibration. It can be seen that the frequencies in Figure 5.12 correspond well with the frequencies determined in the free vibration tests described above.

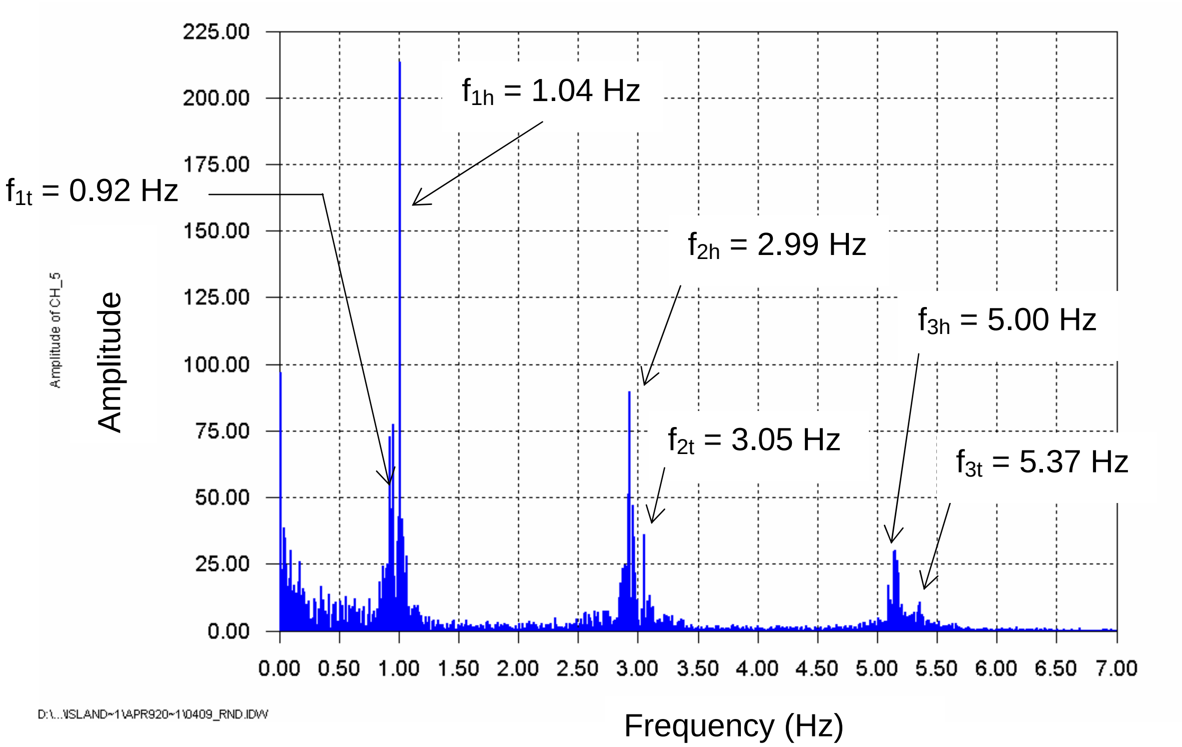

Figure 5.12 – Frequency spectrum for uncontrolled load tests of CH_5
(Note subscript "t" refers to torsional mode, "h" refers to hatcheting mode)
(Island and SR 291)

5.3 Summary of Results

The following conclusions can be drawn from the results of dynamic testing presented above for the two cantilevered mast-arm installations.

1. These structures possess low damping. Damping for the hatcheting mode is around 1% while the torsional mode has damping of approximately 1.5-2.5%. When excited, the structures will experience a larger number of stress cycles than typical steel structures with higher levels of damping. If the stress range of the cycles are large enough, significant fatigue damage could result. The results of the field monitoring will reveal the magnitude and number of stress cycles accumulated during normal wind events.
2. The cantilevered mast-arm structures have two major modes of vibration (torsional and hatcheting), with harmonics of each. The first three torsional and hatcheting modes appear to be the most dominant in the response.
3. The first three modes have frequencies of approximately 1, 3, and 5 Hz, for both structures.
4. Comparison of calculated displacements (by double integration and filtering of acceleration data) with directly measured displacements yields very good correlation.
5. Ambient wind excites both hatcheting and torsional modes of vibration for both structures.

6.0 Results of Long-term Monitoring

The results of the long-term monitoring are discussed in this section. Each pole was monitored for a period of approximately 9 months, from April 1, 2002 through January 3, 2003. During this period, data from selected strain gages and wind speed/direction were recorded. Stress range histograms were developed utilizing the rainflow cycle-counting method. Stress time-histories were recorded when predefined wind speeds were exceeded. Wind speed and direction were recorded every minute. Data were retrieved remotely from the ATLSS lab utilizing a wireless modem every two hours.

6.1 Wind Monitoring

Average and maximum wind speeds were recorded every minute. Average wind directions was also recorded each minute. Using these data, trends can be observed in the wind at the site, such as prevailing wind direction, and magnitude of prevailing winds. Data from each site will be presented separately.

6.1.1 84th and Lindbergh

A plot of the average and peak daily wind speeds for the pole at 84th and Lindbergh is shown in Figure 6.1. It can be seen that the peak wind speed recorded during the monitoring period was 46 mph recorded on April 11, 2002. The wind speed regularly exceeds 20 mph but rarely exceeds 40 mph.

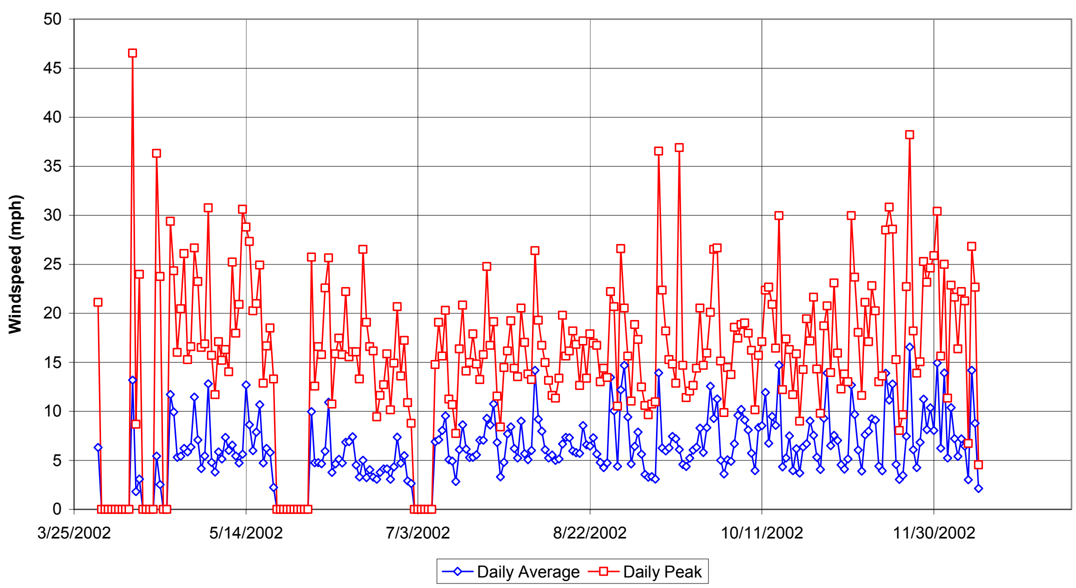

Figure 6.1 – Summary of average and peak daily wind speed for the pole at 84th and Lindbergh

Figure 6.2 contains a three dimensional histogram (also known as a surface plot) of 5 minute average wind speed and direction. It can be seen from this plot that certain wind directions prevail as expected. The prevailing direction appears to be at approximately 90 degrees.

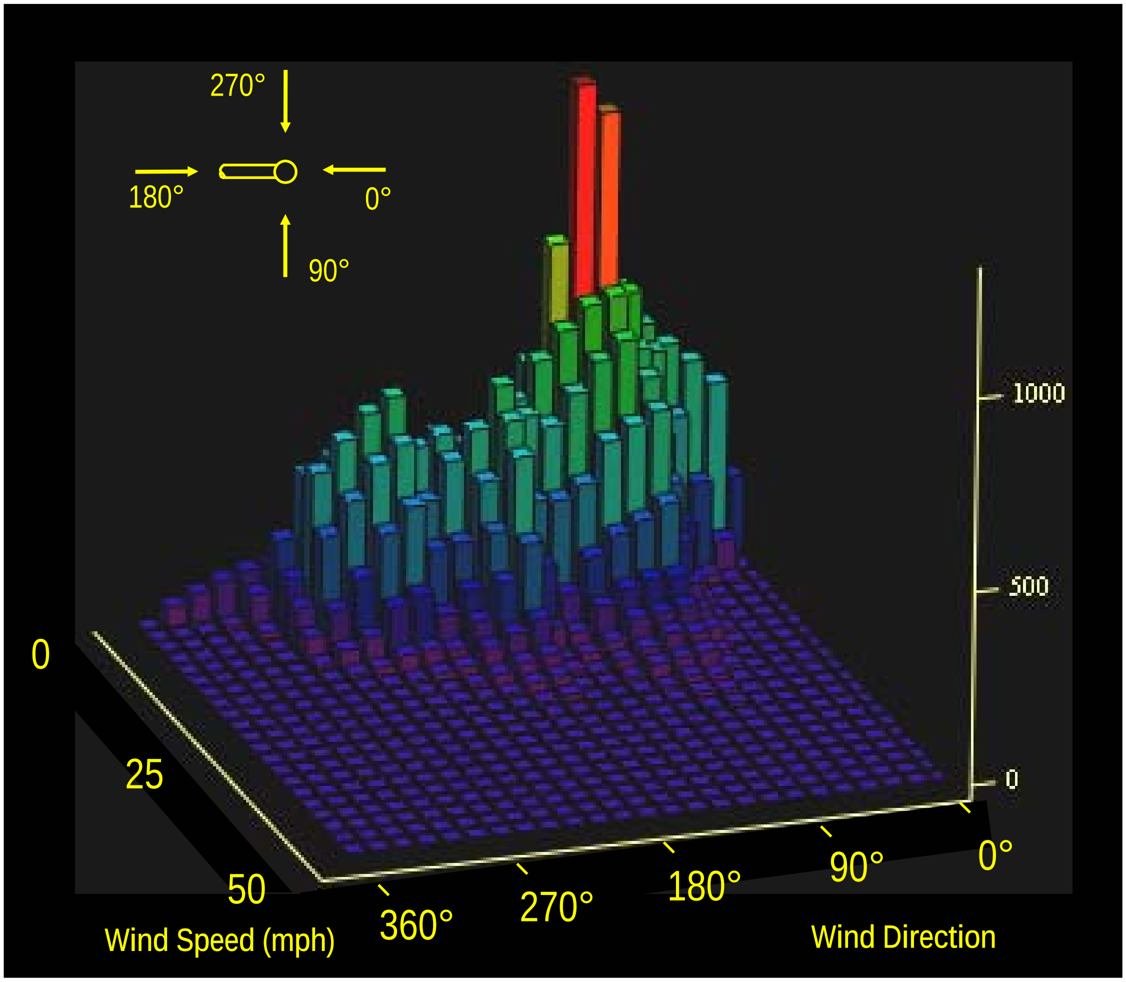

Figure 6.2 - 3D histogram of 5 minute average wind speed and direction for the pole at 84th and Lindbergh

This is further demonstrated in Figure 6.3 which shows a polar histogram plot. This plot shows the percent occurrence of winds from all directions in polar form. It indicates that most of the time the wind direction is 90 degrees, perpendicular to the mast arm.

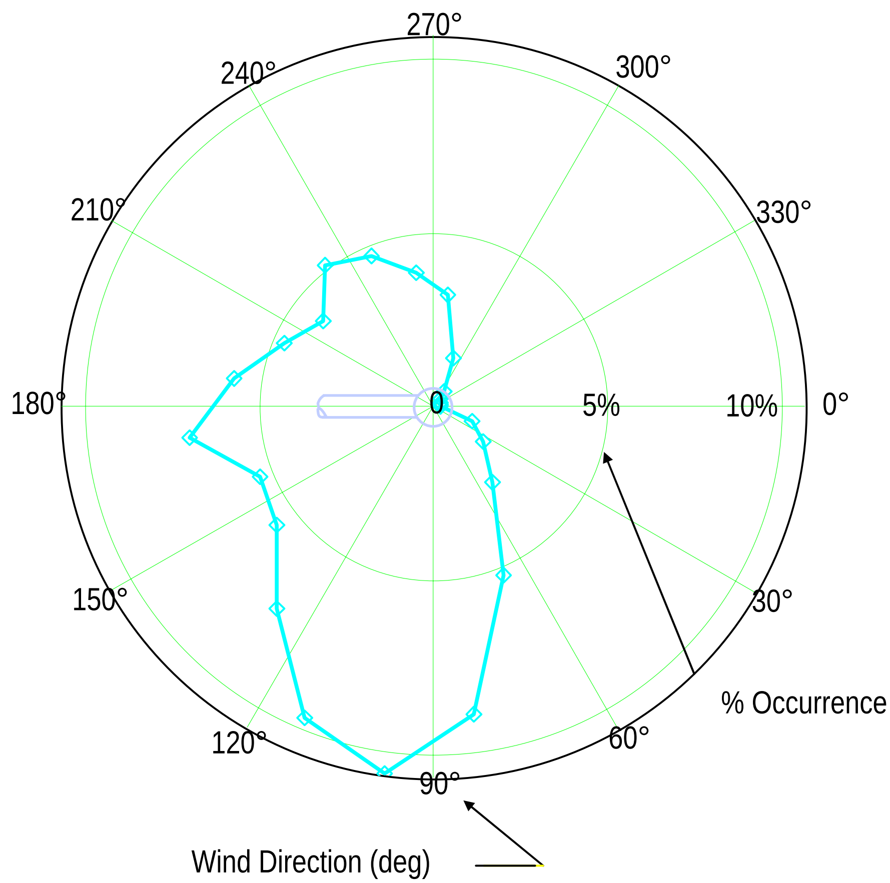

Figure 6.3 – Polar wind direction histogram for the pole at 84th and Lindbergh

Figure 6.4 shows a polar plot of the average wind speed. This plot presents the average wind speed at each direction. It can be seen that the highest average wind speeds of 10 mph are at 180 degrees (parallel to the pole) however, high average winds also exist at 90 and 240 degrees (perpendicular to the pole).

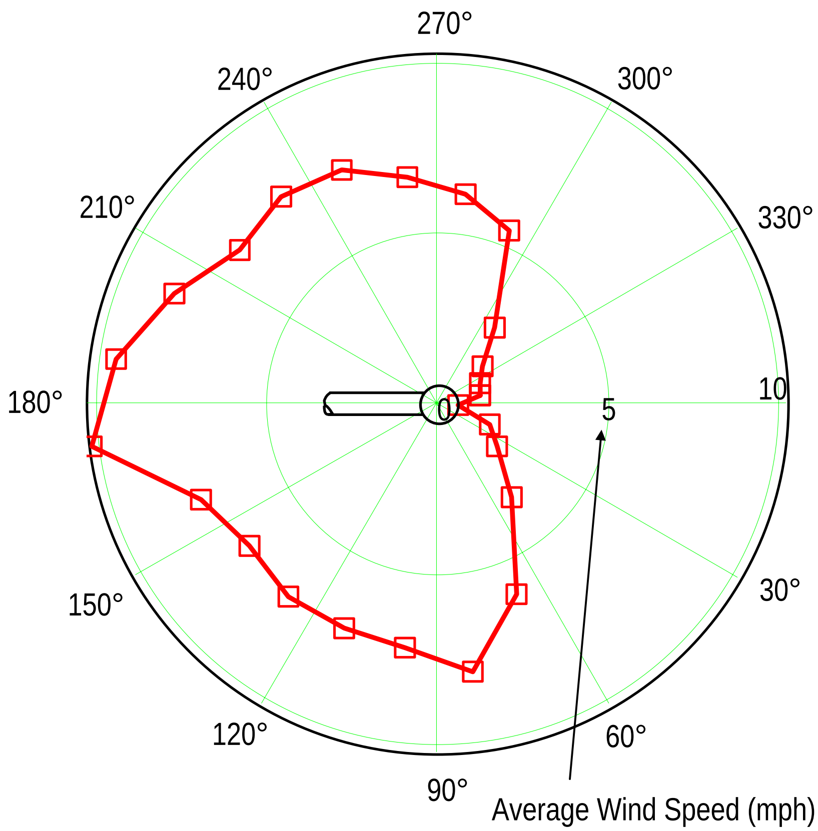

Figure 6.4 - Polar plot of average wind speed versus direction for the pole at 84th and Lindbergh

6.1.2 Island and SR 291

A plot of the average and peak daily wind speeds for the pole at Island and SR 291 is shown in Figure 6.5. It can be seen that the peak wind speed recorded during the monitoring period was 54 mph recorded on November 23, 2002. Again, the peak daily wind speed regularly exceeds 20 mph but rarely exceeds 40 mph. Furthermore, the observed wind speeds at this pole were higher than those at 84th and Lindbergh. This is due to the more open terrain found at the intersection of Island Avenue and SR 291.

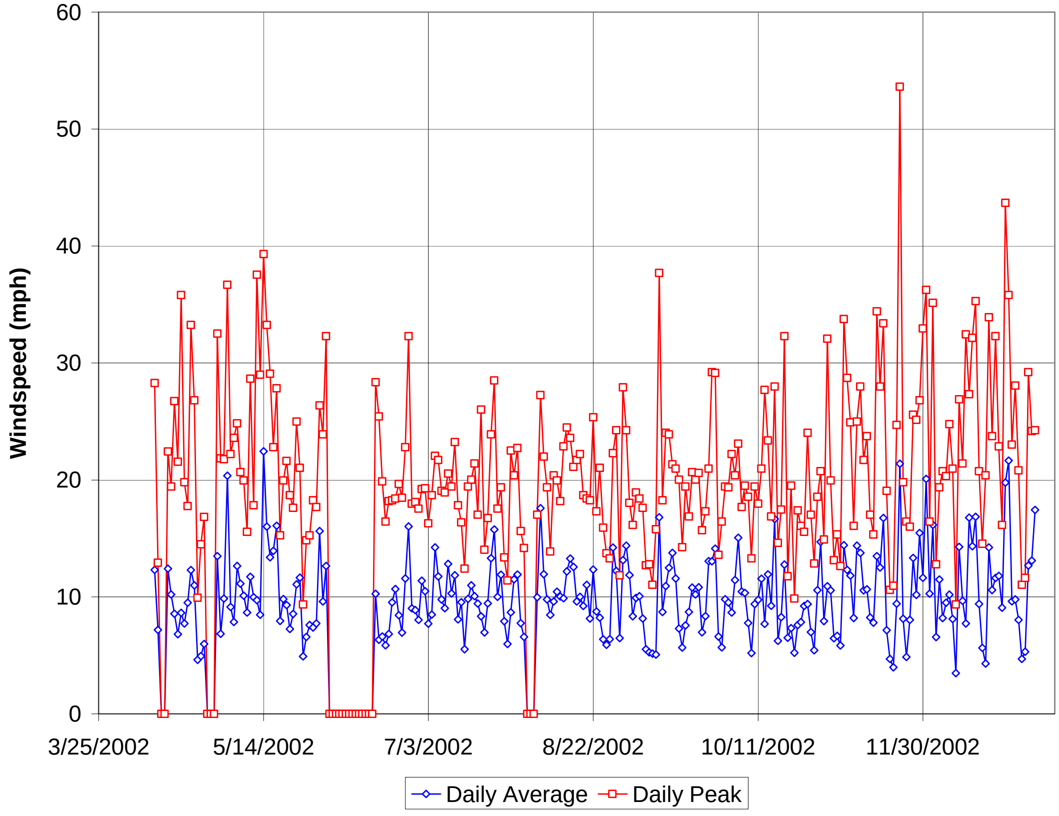

Figure 6.5 - Summary of average and peak daily wind speed
for the pole at Island and SR 291

Figure 6.6 contains a three dimensional histogram of 5 minute average wind speed and direction for the pole at Island and SR 291. As before, the prevailing wind directions can be seen as peaks on this plot.

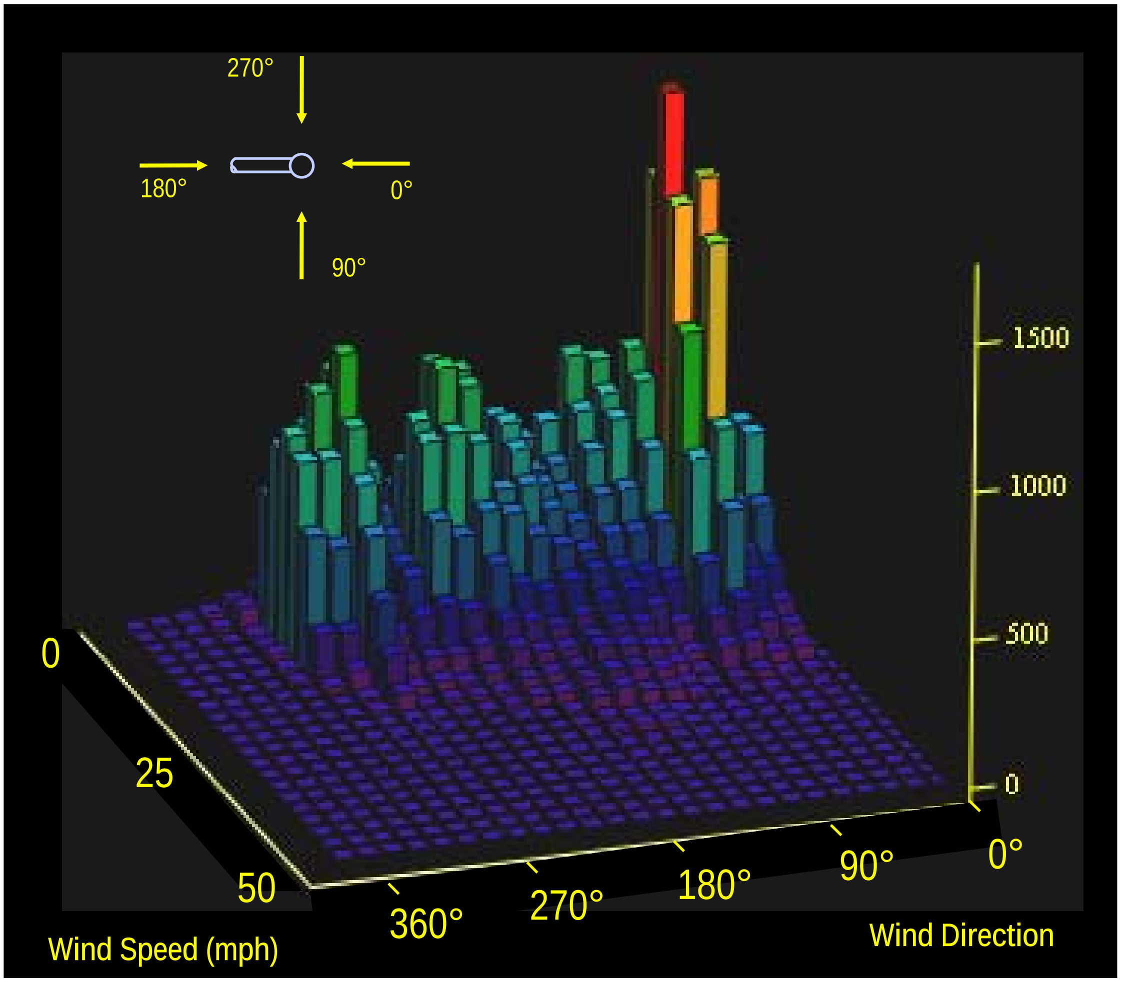

Figure 6.6 – 3D histogram of 5 minute average wind speed and direction for the pole at Island and SR 291

Figure 6.7 contains the polar wind histogram for the pole at Island and SR 291. The prevailing wind at this pole is at 60 degrees, which is nearly perpendicular to the pole and would therefore apply wind loads to the mast arm.

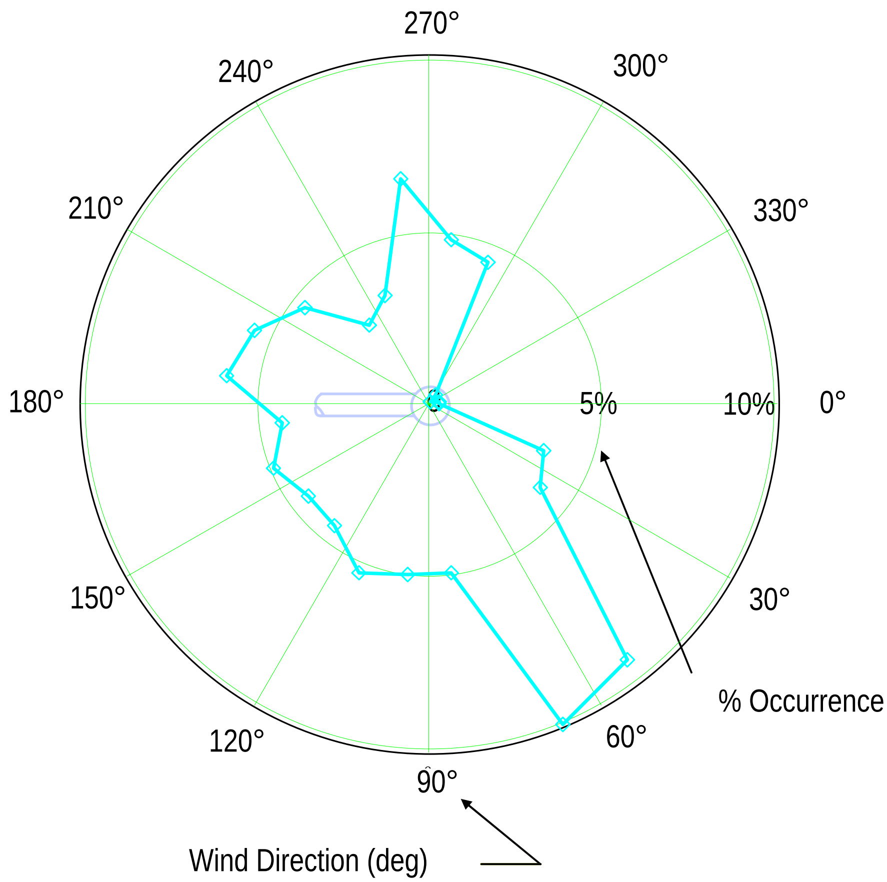

Figure 6.7 – Polar wind direction histogram for the pole at Island and SR 291

Figure 6.8 shows a polar plot of the average wind speed for the pole at Island and SR 291. It can be seen that the highest average wind speeds of 10-12 mph occur fairly uniformly between 30 and 270 degrees. Peak values occur at 50 and 135 degrees.

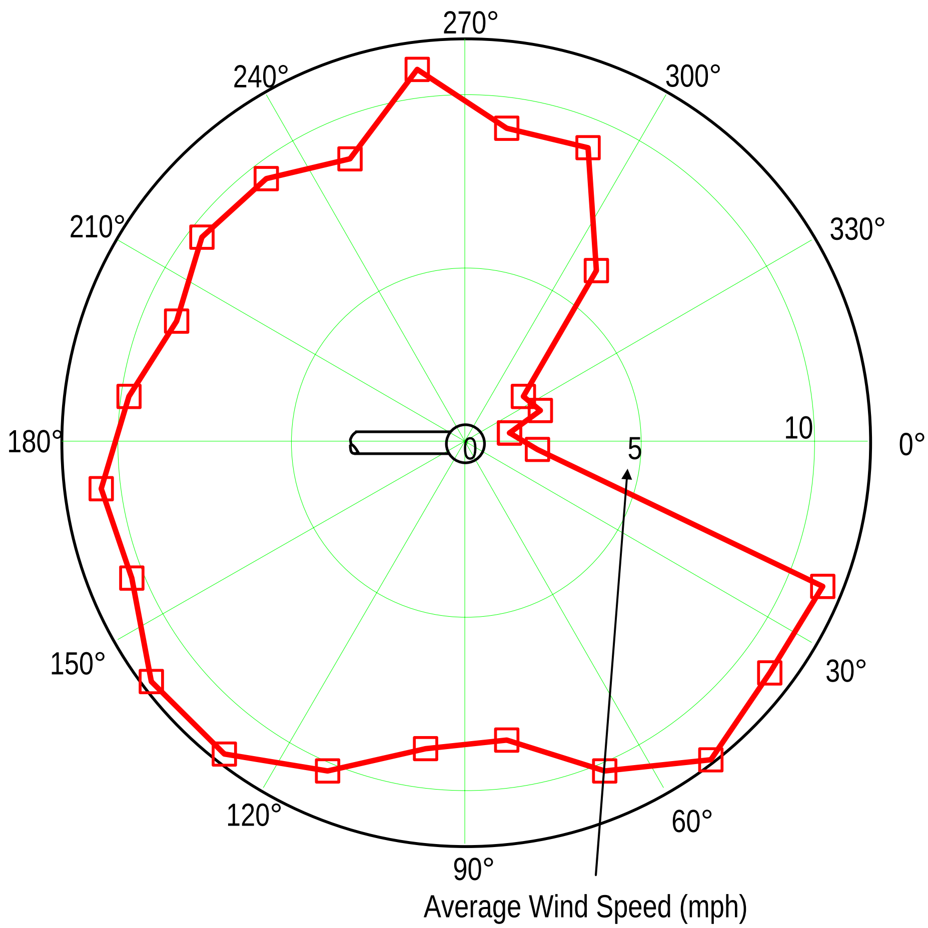

Figure 6.8 – Polar plot of average wind speed for the pole at Island and SR 291

6.2 Stress-range Histograms

As discussed previously, ten strain gages at 84th and Lindbergh, and nine strain gages at Island and SR 291 were selected for long term monitoring. Stress-range histograms were developed for each gage location using the rainflow cycle-counting method. This algorithm converts a block of continuous time-history data (in this study equal to 10 minutes) from a particular strain gage and converts it into a histogram of stress ranges in predefined bin sizes (in this study equal to 0.5 ksi each). The histograms from each of these 10 minute blocks are added together to determine the overall stress range histogram for that gage for the entire monitoring period. Based on the fatigue category of the detail in question, a certain lower-bound stress-range truncation level is selected. Thus, stress cycles below this stress level are neglected in the analysis. The truncation level is selected to be approximately 1/4 to 1/3 of the CAFL of the detail. Using these truncated data, the effective stress range is determined. Finally, estimates of the cumulative damage and remaining fatigue life can be made.

The socket connections (both the shaft-to-baseplate and mast-arm-to-shaft connections) are classified as AASHTO category E', with a CAFL of 2.6 ksi. The box connection at the mast-arm-to-shaft interface is also classified as category E'. A truncation level of 0.5 ksi was used for all gages. The results for each pole are presented and discussed separately below.

6.2.1 84th and Lindbergh

Table 6.1 contains a summary for the 84th and Lindbergh pole of the maximum stress range, effective stress range, number of cycles per day, and an estimate of the remaining life in years based on data from each strain gage. As can be seen, at all locations, the remaining life is estimated to be at least greater than 50 years, despite the fact that the CAFL was exceeded at some locations with a frequency of greater than 1/10,000 (or 0.01%).

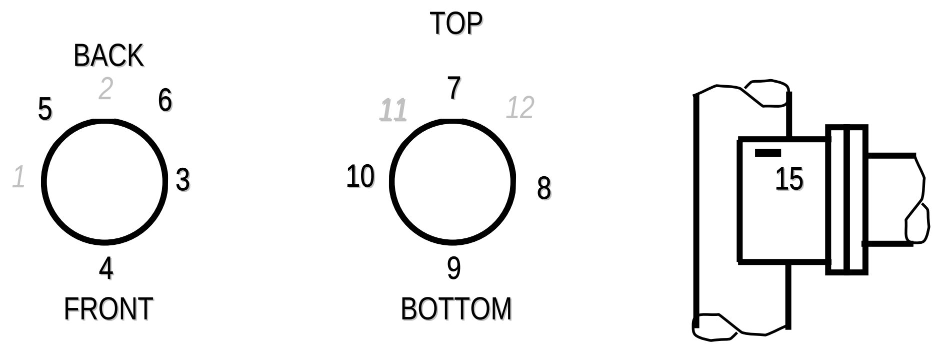

Location	Strain Gage	S_{rmax} (ksi)	Cycles > CAFL		S_{reff} (ksi)	Cycles/ day	Remaining Life (years)
			#	%			
shaft-to-base	CH_3	1.5	0	0.00%	0.76	20	infinite
	CH_4	2	0	0.00%	0.77	40	infinite
	CH_5	1.5	0	0.00%	0.76	20	infinite
	CH_6	4	58	0.04%	0.86	580	>50
mast-to-shaft	CH_7	5	333	0.16%	0.91	950	>50
	CH_8	3.5	87	0.04%	0.89	880	>50
	CH_9	6	814	0.46%	0.99	780	>50
	CH_10	3	22	0.02%	0.85	620	>50
	CH_15	7	1031	0.64%	1.02	720	>50

Table 6.1 – Summary of stress range histograms for the pole at 84th and Lindbergh

6.2.2 Island and SR 291

Table 6.2 contains a summary for the Island and SR 291 pole of the maximum stress range, effective stress range, number of cycles per day, and an estimate of the remaining life in years based on data from each strain gage. As can be seen, at all locations, the remaining life is estimated to be at least greater than 50 years, despite the fact that the CAFL was exceeded at some locations with a frequency of greater than 1/10,000 (or 0.01%).

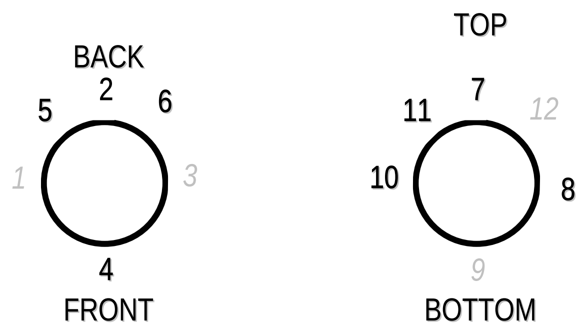

Location	Strain Gage	S_{rmax} (ksi)	Cycles > CAFL #	Cycles > CAFL %	S_{reff} (ksi)	Cycles/ day	Remaining Life (years)
shaft-to-base	CH_2	1.0	0	0.00%	0.75	20	infinite
	CH_4	1.0	0	0.00%	0.75	0	infinite
	CH_5	3.5	4	0.00%	0.79	740	infinite
	CH_6	4.0	110	0.07%	0.83	760	>50
mast-to-shaft	CH_7	3.0	5	0.01%	0.81	390	infinite
	CH_8	5.0	556	0.06%	0.87	4230	>50
	CH_10	7.0	412	0.07%	0.85	2640	>50
	CH_11	2.5	0	0.00%	0.78	760	infinite

Table 6.2 – Summary of stress range histograms for the pole at Island and SR 291

6.3 Summary of Findings – Long-term Monitoring

Based on the data and results from the long-term monitoring presented above, the following conclusions can be drawn.

1. Wind speeds at both poles regularly exceed 20 mph
2. Wind speeds at both pole rarely exceed 40 mph
3. The maximum wind speed recorded at either pole during the nine month monitoring period was 54 mph.
4. Higher wind speeds were recorded at the pole at the intersection of Island Avenue and SR 291 due to the more open terrain found there.
5. In general, maximum wind speeds and prevailing winds are at a direction perpendicular to the mast arm.
6. Low effective stress ranges (generally less than 1 ksi) were measured at the mast-arm-to-shaft and shaft-to-base connections at both poles. All effective stresses were less than the CAFL of 2.6 ksi (for category E').
7. The CAFL was exceeded at some locations on both the mast-arm-to-shaft and shaft-to-base connections. In some cases the frequency of exceedence was greater than 1/10,000 (or 0.01%), which indicates that finite fatigue life can be expected.
8. At all instrumented locations, either infinite life is expected (stress ranges greater than the CAFL occurred with a frequency of less than 1/10,000) or the calculated finite life is greater than 50 years, which is most likely greater than the remaining functional life of these structures.

APPENDIX A

Instrumentation Plans
Cantilevered Mast-arm Structures at:

84th St. and Lindbergh Blvd.

Island Ave. and SR 291

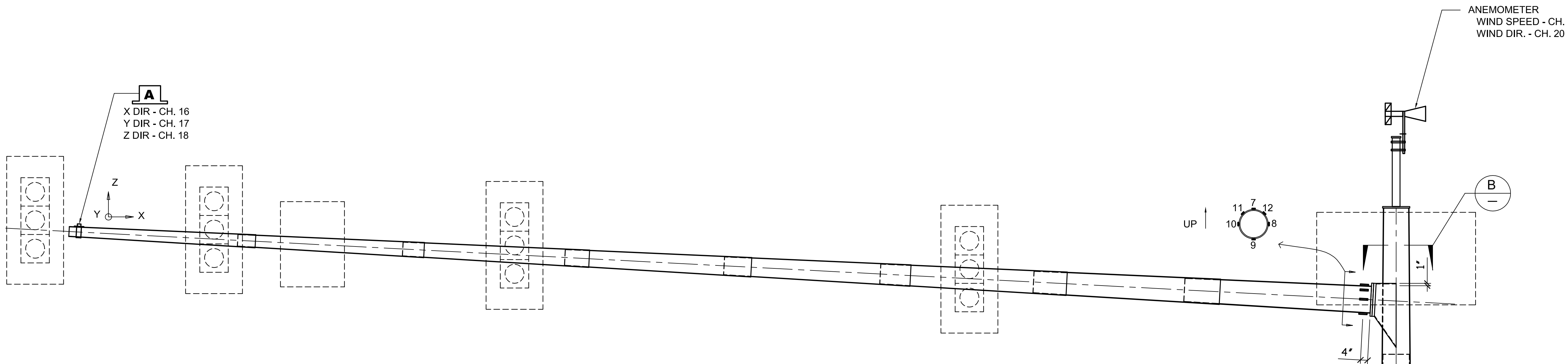

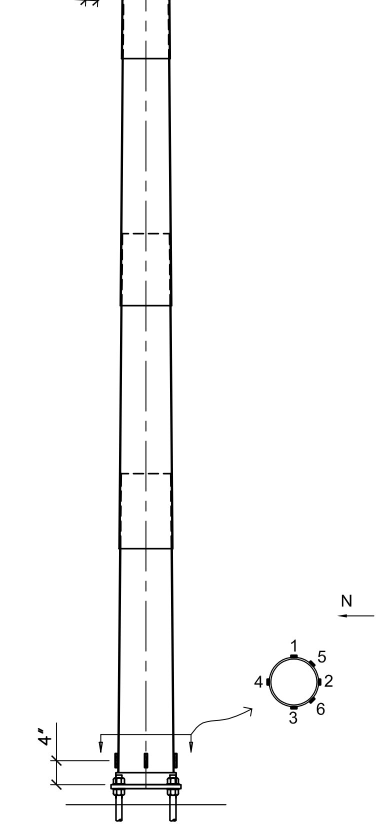

ELEVATION LOOKING EAST
1/4" = 1'-0"
A

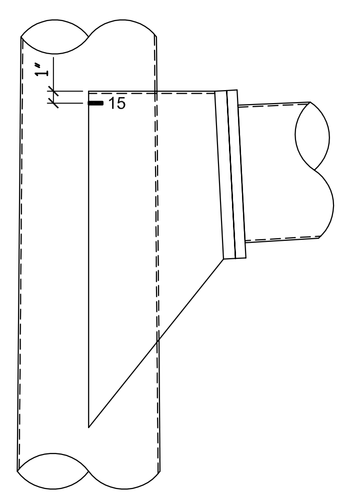

SECTION C
3/4" = 1'-0"

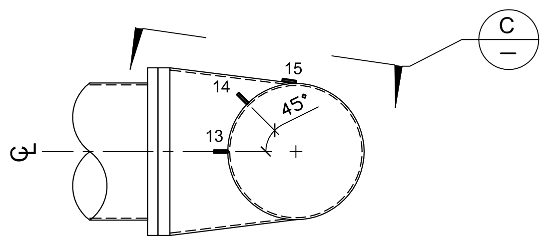

SECTION B
3/4" = 1'-0"

LEGEND

A = ACCELEROMETER (TOTAL = 1 UNIT, 3 CHANNELS)

= STRAIN GAGE (TOTAL = 15)

ADVANCED TECHNOLOGY FOR
LARGE STRUCTURAL SYSTEMS
117 ATLSS Drive
Lehigh University
Bethlehem, PA 18015
610-758-3500 FAX 610-758-5553

PROJECT:

CITY OF PHILADELPHIA MAST ARM EVALUATION

SHEET NOTES:

1. ALL DIMENSIONS SHOWN SHALL BE VERIFIED IN FIELD.
2. STRAIN GAGES SHALL BE PLACED ADJACENT TO WELD TOE, UNLESS OTHERWISE NOTED.
3. DIMENSIONS GIVEN FOR STRAIN GAGE LOCATIONS ARE MEASURED FROM THE WELD TOE.

NO.	DESCRIPTION	DATE	BY
2	AS INSTALLED	3/14/02	ICH
1	INITIAL PLAN	2/11/02	ICH

DESIGNED BY:	ICH
DRAWN BY:	ICH
CHECKED BY:	ICH
SCALE:	AS NOTED
DATE:	2/11/02
PROJECT NO.:	
SHEET TITLE:	

INSTRUMENTATION PLAN - 84TH ST. & LINDBERGH BLVD.

SHEET NO.:

1 OF 2

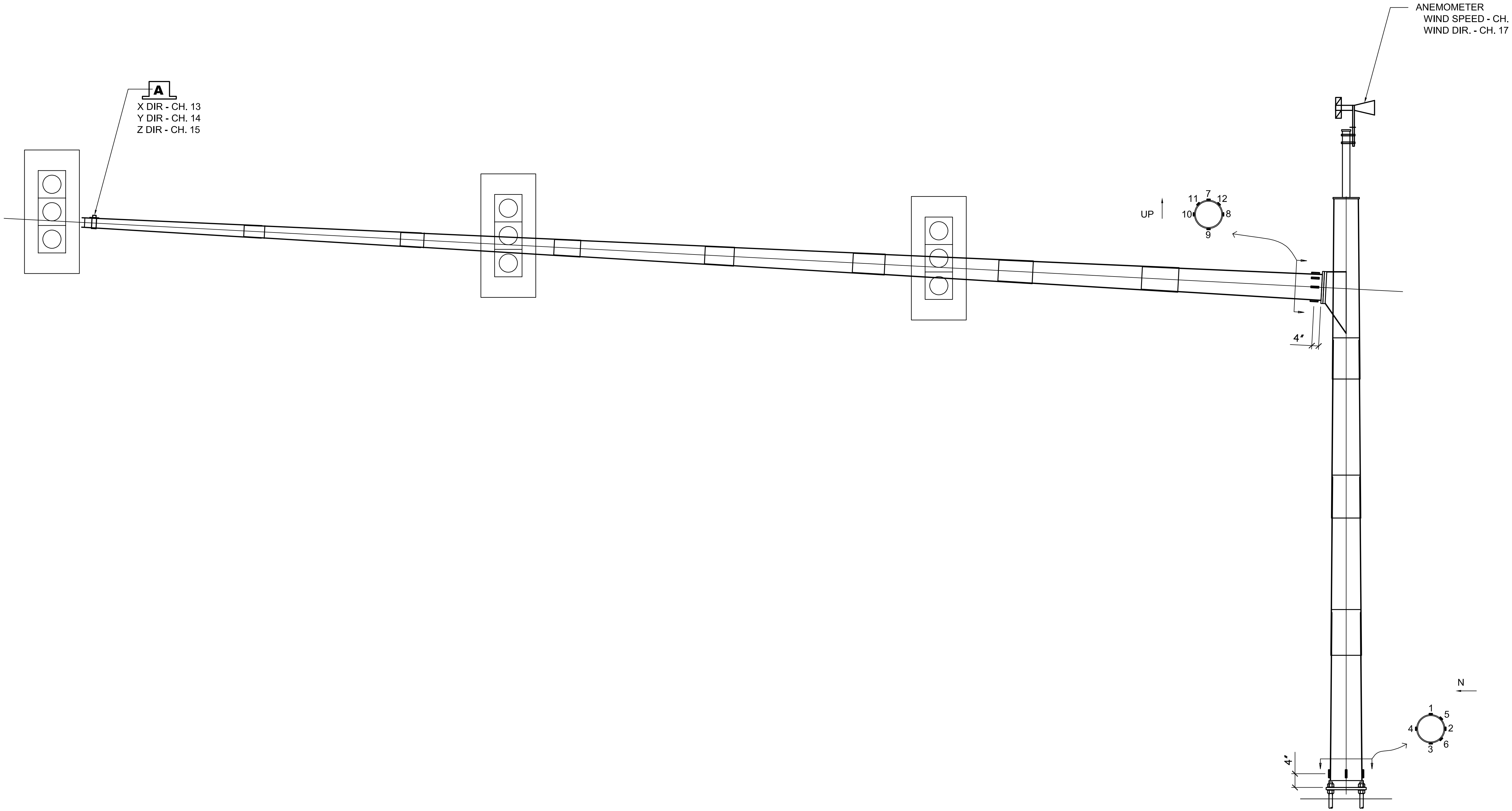

ELEVATION LOOKING EAST

1/4" = 1'-0"

A

LEGEND

A = ACCELEROMETER (TOTAL = 1 UNIT, 3 CHANNELS)

= STRAIN GAGE (TOTAL = 12)

ATLSS

ADVANCED TECHNOLOGY FOR LARGE STRUCTURAL SYSTEMS
117 ATLSS Drive
Lehigh University
Bethlehem, PA 18015
610-758-3500 FAX 610-758-5553

PROJECT:

CITY OF PHILADELPHIA MAST ARM EVALUATION

SHEET NOTES:

NO.	DESCRIPTION	DATE	BY
1	INITIAL SUBMITTAL	2/11/02	ICH

DESIGNED BY:	ICH
DRAWN BY:	ICH
CHECKED BY:	ICH
SCALE:	AS SHOWN
DATE:	2/11/02
PROJECT NO.:	
SHEET TITLE:	

INSTRUMENTATION PLAN - ISLAND AVE. & SR291

SHEET NO.:

APPENDIX B

Destructive Evaluation

B.1 Introduction

The ATLSS Engineering Research Center was contracted by the consulting firm of Edwards & Kelcey to conduct field testing and destructive laboratory investigation on cantilevered signal support structures in the City of Philadelphia, Pennsylvania. The results of the destructive evaluations on various mast-arm components are discussed in this section. The destructive evaluation is only a small component of a larger program conducted by the City to evaluate the condition of its aging cantilevered signal structures. The effort also includes extensive field instrumentation, monitoring, inspection, and analysis. The lack of structural redundancy of cantilevered signal support structures combined with their location over active traffic lanes requires careful evaluation of the existing condition of these structures.

Destructive evaluation can be used to minimize speculation as to the level of in-service damage that has occurred to the structure. Destructive evaluation is one method that may also be used immediately after fabrication to verify weld quality. When weld conditions can be carefully controlled, or when welds are repetitive and uncomplicated it may be more practical to use non-destructive testing methods to verify weld quality. AASHTO's Standard Specifications for Structural Supports for Highway Signs, Luminaries, and Traffic Signals in article 5.15.3 requires random non-destructive testing of 25% of all baseplate and endplate connections. AASHTO also allows for destructive testing to be used in place of non-destructive testing as acceptable to the owner (Reference A). Destructive evaluation may even be more important as the structure nears the end of the design life. Destructive evaluation techniques, combined with traditional inspection procedures may be used to evaluate the current and future safety of the structure, plan a replacement program, and possibly extend the design life of the structure.

It is important to note that the conclusions of a destructive evaluation can provide valuable insight to the future performance of the structure, but may not override safety provisions set fourth by AASHTO or any other applicable design code. The utilization of a destructive or non-destructive evaluation program in conjunction with field-monitoring of in-service stresses provides an excellent method to quantify the “health” of an aging infrastructure.

Destructive evaluation of a representative number of the City of Philadelphia’s cantilever signal support structures can provide valuable information related to the condition of the inventory. However it is critical to obtain a representative group of samples. The number of stress cycles a cantilevered signal support structure will experience is greatly affected by many factors including: The local weather conditions including the frequency of high speed wind and the wind direction, and the response characteristics of the structure. These factors affecting the stress history of cantilevered signal support structures can vary greatly depending on location.

The objective of the destructive evaluation was to detect any defects in the welded joints. By noting the occurrence and magnitude of weld defects in the specimens examined, the weld quality of similar cantilevered signal support structures can be estimated. Structural weld defects can be divided into two groups. The first is the result of in-service weld defects, which are the result of cyclic loading and fatigue crack initiation and growth. The second group represents “flaws” that were “built into” the structure. These flaws are typically as-fabricated weld defects, which occurred during or shortly after fabrication.

The American Welding Society notes the difficulty in precisely defining weld quality and indicates that precise definitions are specified in design codes. The AWS begins its definition of weld quality by using the term fitness for purpose. This term expands the definition of weld quality, as the most skillfully fabricated weld which will not meet functionality requirements if it was designed incorrectly. The AWS further states that safety is not the only consideration. Economics must also be considered when choosing the desired level of weld quality. In order to approach this balance of safety and economics, the AWS mentions the importance of sound engineering judgment in interpreting and meeting the minimum levels of weld quality, as well as the importance of non-destructive testing. The final remark on the definition of weld quality made by the AWS details the means by which physical characterizations of weld quality are made and the absolute importance of “understanding the occurrence, examination, and correction of any [weld] defects” (Reference B).

However, in the context of this investigation weld quality is characterized with the level of penetration and completeness of fusion. The destructive evaluation was not limited to these two parameters, but also considered other types of weld defects including slag inclusion, under cut welds, porosity and cracking. Lack of fusion and incomplete penetration are likely to be present to some degree even if the welded joint quality is adequate. Both of these defects can form transverse to the applied stress, creating an initiation point where fatigue cracking will begin under cyclic stress ranges.

B.2 Description of Specimens

The ATLSS Engineering Research Center received a total of ten (10) individual specimens of sign signal structures. The specimens were either a base plate to column connection or a column to mast-arm connection. The specimens were obtained from the City of Philadelphia without documentation regarding the respective orientation of the mast-arm on the base plate. Three of the structures were taken out of service because of damage sustained due to vehicle impact. Four complete cantilevered signal support structures, consisting of both a base plate to column and a column to mast-arm connection were obtained from Arrugut and Walnut, Old Bustleton Avenue and Walsh, Castor and Wingohocking South West corner, and Castor and Wingohocking North East corner. Another base plate to pole specimen was obtained from Broad and 70th street.

Outer Ring

Figure 1. Baseplate Sample 1

Figure 2. Typical hand Access hole

A total of five base plate samples were received. These samples were labeled as samples B-1 through B-5 after arriving to the laboratory. These samples included the base plate to column connection and approximately 3 feet of column length, which included the hand access hole. The base plate dimensions of these 5 specimens ranged from a square 16 11/16” by 1 1/16” thick (sample B-1 seen in Figure 1), to 14” square with a thickness of 3/4” (sample B-4). The hand access hole dimensions were typically 4” by 10”, located tangent to the square base plate, approximately 12” above the base plate, as seen in Figures 1 and 2. One key feature of the base plate to column connection is the use of an outer ring to reduce the stress in the welded joints of the base plate to column connection (as seen in Figure 1).

Due to the lack of documentation, the orientation of the base plate specimens relative to the mast-arm is unknown. However according to a City of Philadelphia engineer, approximately 90% of all cantilevered signal structures are oriented with the hand access hole directed away from the roadway, hence on the opposite side of the mast-arm. This would put the tension stress due to the deadweight moment of the mast-arm on the side of the hand access hole. The seam of the column tube was always positioned along the neutral axis of the tube, 90° from the hand access hole. In samples B-1 through B-4, the seam was positioned 90° clockwise in plan from the hand access hole, and in sample B-5 the seam was positioned 90° counter-clockwise in plan from the hand access hole. Also, base plate samples B-2, B-3, and B-4 were all manufactured by Poles Inc., indicated by a sticker placed above the hand access hole. It is not known who fabricated the other specimens.

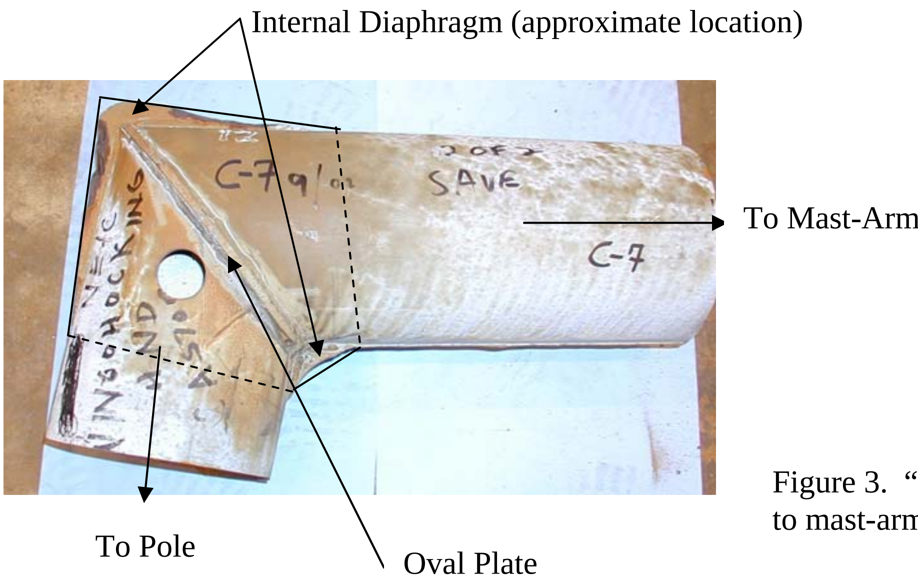

Figure 3. “Corner Style” column to mast-arm connection.

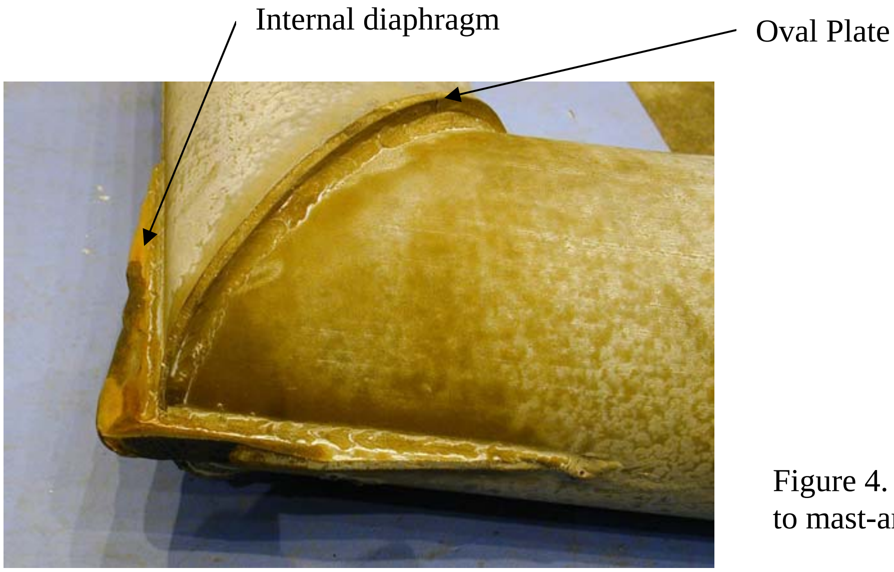

Figure 4. Corner style column to mast-arm connection detail.

Three corner or elbow style column-to-mast-arm connections were obtained. These specimens were labeled as C-6 through C-8. These connections are characterized by a complicated geometry consisting of approximately a 95° to 100° intersection of the pole and the mast-arm (Figure 3). The three dimensional geometry of these samples can be conceptualized by visualizing the column and mast-arm cut at 50° angles and joined together at an oval plate. Because both the mast-arm and column are made of thin steel tubes; this connection would be susceptible to buckling. In order to prevent this, an internal diaphragm is inserted to help transfer the vertical shear force from the mast-arm to the column and to prevent the joint from buckling.

The first step in fabrication of a corner styled column to mast-arm connection is creating the internal diaphragm assembly. The internal diaphragm is constructed by bisecting an oval plate with a large central circular hole and a smaller diameter hole above and along the long direction of the oval (Approximate diameters 4" and 2" respectively as seen in Figure 5). These half ovals are then fillet welded to the "L" shaped diaphragm on each side completing the internal diaphragm. The column and mast-arm are then cut at 50° angles and slotted to allow for the portion of the internal diaphragm that will stick out. The final step is to fillet weld the column and mast-arm to both the internal diaphragm and the oval plate plate. Figure 4 is a photograph of these external fillet welds. Figure 5 is a graphic model illustrating the internal diaphragm assembly.

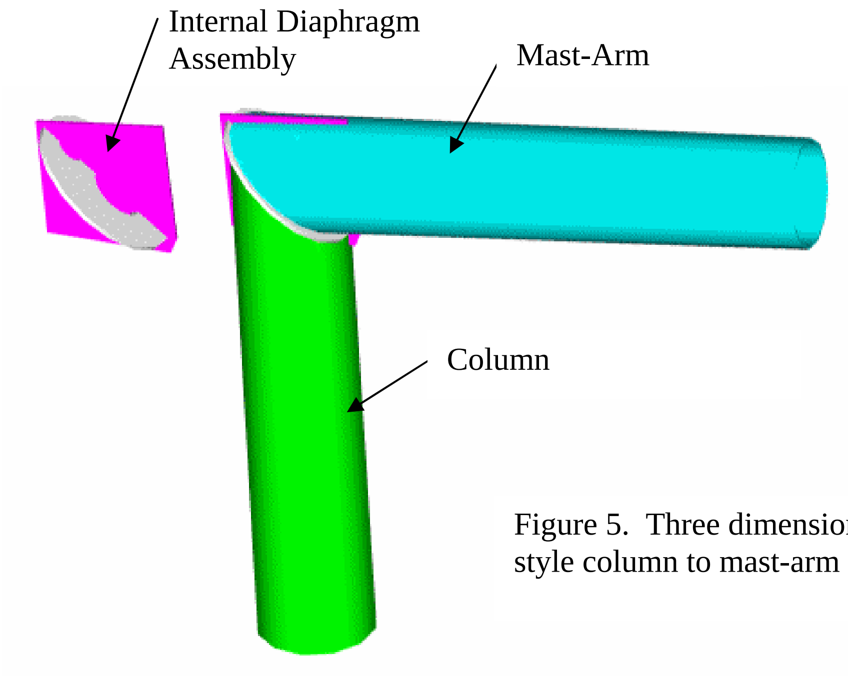

Figure 5. Three dimensional model of corner style column to mast-arm connection detail.

The vertical orientation of the corner samples was easily determined by water drip mark patterns, and the fact that both the column and mast-arm are tapered.

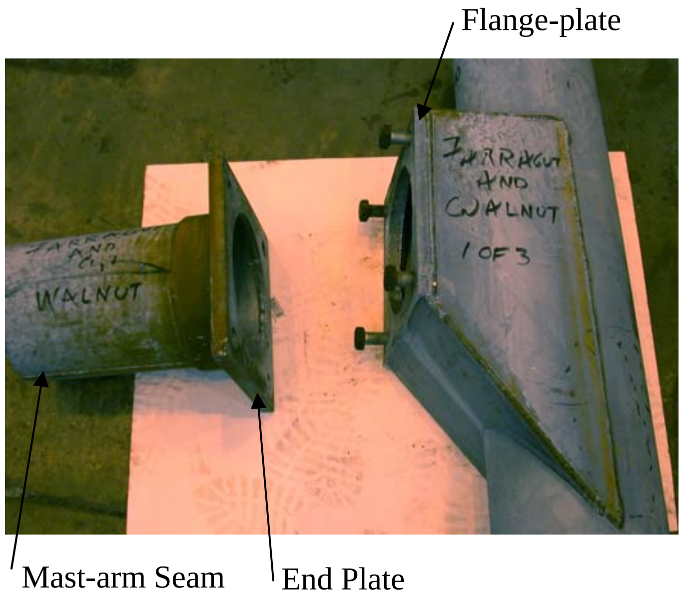

Figure 6. Bolted Flange plate style column to mast-arm connection.

One complete bolted endplate style column to mast-arm connection was obtained (See Figure 6). The endplate portion of the connection consisting of the mast-arm side of the mast-arm to column connection was labeled as specimen E-9. The large built-up box fixture, which the endplate is bolted onto, was labeled as E-10 (See Figure 6).

The mast-arm endplate, specimen E-9, is very similar to the base plate detail discussed earlier, only scaled down. The only significant difference is the lack of a hand access hole. The tension side of the mast-arm endplate specimen was determined by identifying the direction of water drip stains. The water drip pattern suggested that the seam of the mast-arm tube was on the bottom of the mast-arm, hence in compression.

The built-up box is constructed of a ¾” steel plate or flange plate as shown in Figure 6. The rest of the flange box is constructed with 3/8” thick steel plates. The built-up box, which is slightly wider than the diameter of the column, is cut out to conform to the circular column. This difference in widths creates a very long vertical weld of questionable quality, as well as complicated non-perpendicular box geometry. The entire perimeter of the intersection of the column and the flange box is fillet welded as shown in Figure 6.

B.3 Documentation of Initial Condition/Damage

The specimens were first visually inspected to document their initial condition. The visual inspection specifically focused on geometric flaws such as bent or out of straight joints, surface flaws such as deterioration of the surface finish and signs of oxidation, and weld defects including cracks, undercut welds, spatter, and porosity. The majority of the visible surface damage discovered was due to vehicular impact, and seen in the base plate to column specimens. One corner style column to mast-arm connection was also dented, most likely during removal or transport. The surface examination revealed only one instance of a visible surface weld defect, which was not the result of vehicle impact or demolition.

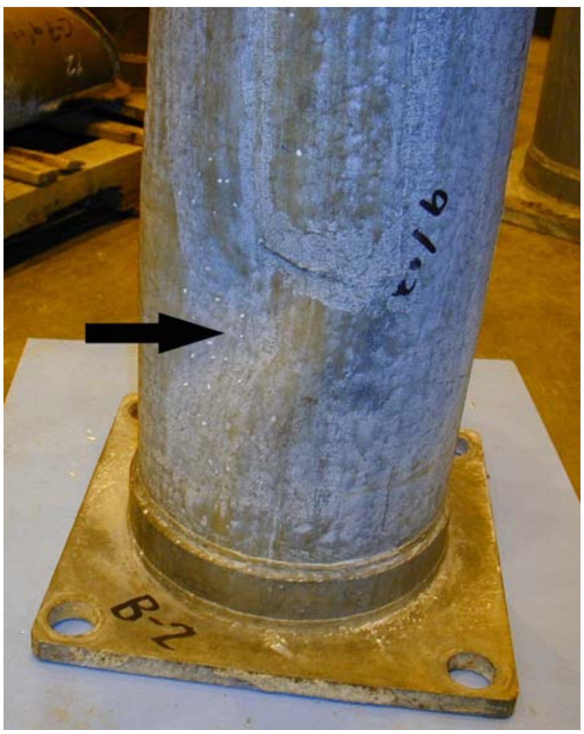

Figure 7. Damage typical to Samples B-2 and B-4

Figure 8. Damage to Sample B-5

Baseplate specimens B-2, B-4, and B-5 were damaged by vehicle impacts. Both sample B-2 and B-4 had large dents on the column directly opposite of the hand access hole, the side adjacent to the road. Figure 7 shows the damage to specimen B-2, which is similar to the damage of specimen B-4. Sample B-5 indicated a very severe impact, with significant deformation of the column opposite of the hand access hole, as shown in Figure 8. The fillet welds opposite to the hand access hole were also torn apart by the severe impact.

Column to mast-arm connection specimen C-8 was also severely dented. The dent was located on the bottom of the mast-arm directly at the joint, causing some tearing of the welded connection between the internal diaphragm and the mast-arm tube, as seen in Figure 9. It is believed that the damage was sustained during the removal or shipment of the structure due to the localized nature of the damage. The damage is limited to only the bottom of the mast-arm. As the damage is only on the bottom, it is probable that the damage is a dent resulting from a fall during demolition or transport.

Figure 9. Localized damage to sample C-8

Specimen E-10, (the built-up box specimen) was the only specimen to have any type of visible surface weld defect. Figure 10 shows the location and length of the visible surface crack in the vertical fillet weld joining the built up box to the column. The crack was measured to be approximately six inches long originating one inch from the bottom of the vertical fillet weld.

As discussed earlier, the built-up box weld detail is difficult and awkward to fabricate. The difficulty is primarily due to the complex geometry of the assembly. The complex geometry is caused by the flange plate being approximately one inch wider than the diameter of column. The top and bottom plates of the built up box must be cut to form fit to the column. The sides of the built-up box must be fabricated as to form fit to the column also. During the fabrication of the built up box, tolerances introduced by the manual and custom-built nature of the fabrication vary. As result, there will likely be some small gaps as the built-up box will not fit perfectly to the column. The built up box is fillet welded along the entire perimeter of the built-up box, as shown in Figure 10. The two long vertical fillet welds possess a significant amount of residual stress. As the weld metal of these two vertical fillet welds cools, the weld metal is restricted from contracting due to its bond to the column. This restricted contraction of the weld metal induces the residual stress in the weld. High residual stresses as well as a poor bond between the weld metal and the column surface are the probable contributors to the crack.

Figure 10 – Photograph of upper mast-arm connection

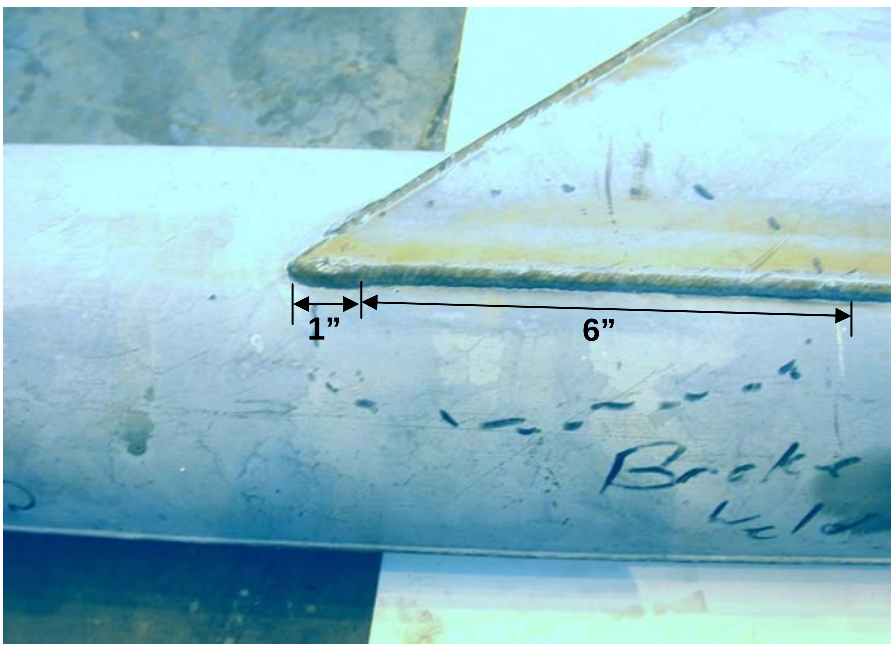

B.4 Destructive Evaluation

B.4.1 Approach

In order to detect any possible fatigue damage, sections were cut through the welded joints. These sections were inspected for fatigue cracking and weld defects. Since fatigue cracks propagate perpendicular to applied tension stress, sections were cut parallel to the applied stress. Because the exact orientation of the specimens was undocumented, sections were taken in both the assumed tension and compression regions of each specimen.

To determine the longitudinal stresses at the welded joints, the cantilevered signal support structure can be idealized as a cantilevered frame member or a cantilevered beam. Thus the longitudinal stresses are given by the bending stress relationship $s = Mc/I$. In the case of the cantilevered signal support structure the moment is produced by the deadweight of the mast- arm and any wind induced vertical disturbance to the mast-arm. The approach of this destructive evaluation is to cut and examine sections through welded joints that experience the greatest tensile stress range. When stress variations are caused by fluctuating moment loading, the maximum tensile stress ranges will occur at the furthest distance away from the neutral axis according to simple beam theory. The three types of welded joints considered are: the baseplate to column connection, the hand access hole fillet welded connection, and the column to mast-arm connection including both corner and endplate style connections.

In the baseplate to column welded connection, the maximum stress experienced by the welded connection would be expected on the tension side of the pole. However, it was observed in the field monitoring program that the maximum stress in the welded baseplate to column connection, occurs radially in line with the centers of the anchor bolts. This behavior is explained by bending which occurs in the baseplate. Hence sections were also cut in line with the anchor bolts. If the baseplate were infinitely rigid the maximum stress would occur at the expected location according to simple beam theory. Sections were cut as shown in Figure 11.

The welded connection between the hand access hole and the column is also another exception to the generality that maximum stress is located at the maximum distance away from the neutral axis. Since the hand access hole is located on the tension side of the column, a stress concentration exists at the corners of the welded connection between the hand access hole and the column. In addition to the central portion of the top and bottom of the hand access hole (the location of maximum distance to the neutral axis), the corners of the hand access hole are also areas of concern for fatigue crack growth. Sections were cut at these locations as shown in Figure 12.

B.4.2 Process

In order to obtain sections through welded joints, which were previously identified as locations of maximum tensile stress, several cuts were made using a Marvel Metal Band Saw No. 8, made by Armstrong-Blum Manufacturing company. Each section produced two samples with mirrored faces through the weld. Both of these faces were finished using mechanical and chemical procedures to produce a smooth finish that would allow for the inspection of cracks. These two faces are not identical since the metal band saw removes approximately 1/16" of material, as well as the material loss that came with the finishing process discussed in detail below. The total width of removed material between the two faces in some case may have been as much as 1/8".

The mechanical or grinding process used to prepare the samples depended on the size of the sample. Corner style column to mast-arm samples were initially ground using grinding wheels, using passes of 120, 160, 200, 240, 300, 400, and 600 grit sanding paper followed by a final pass with a diamond powder grit wheel. Due to their larger size, baseplate samples were first ground using an industrial grinder, with a sand paper grit of 120, followed by a grit of 160. Different chemical etching processes were used on baseplate samples to achieve the surface quality desired. Using a 5% Nitric acid and ethanol or 5% Nital solution, the baseplate samples were chemically etched. The chemical etch smoothes out any roughness left by the coarser sand paper. The baseplate samples were chemically etched for approximately two hours. Because the corner samples were considerably smoother after grinding, the chemical etching process used was less severe. The corner samples were etched with a 2% Nital solution for 30 minutes. Hand access hole and endplate samples were ground and etched in a manner similar to the baseplate samples.

In each baseplate to column connection specimen, eight sections were made as shown in Figure 11. Specifically one cut was made through each corner and through the midpoint of each side, creating a total of 16 samples per baseplate. Because of the unknown orientation of the baseplate, sections were made in both the tensile and compression sides of the specimen. The baseplate samples were numbered using the number system also shown in Figure 11, where side 1 2 marks the tension side of the column and also the hand access hole. Baseplate specimens B-1 through B-4 were also sampled and prepared in this manner. Sampling of specimen B-5, which was significantly damaged in a car accident, was limited to the welded joints which were still intact.

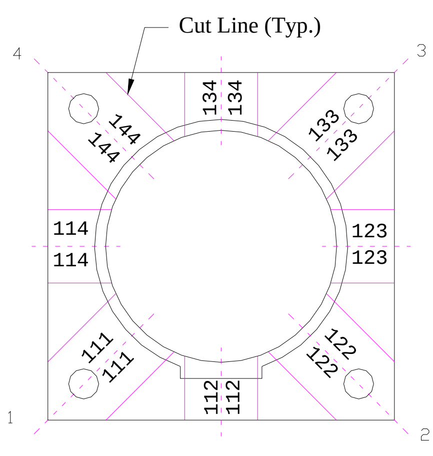

Figure 11.
Baseplate Sample Location

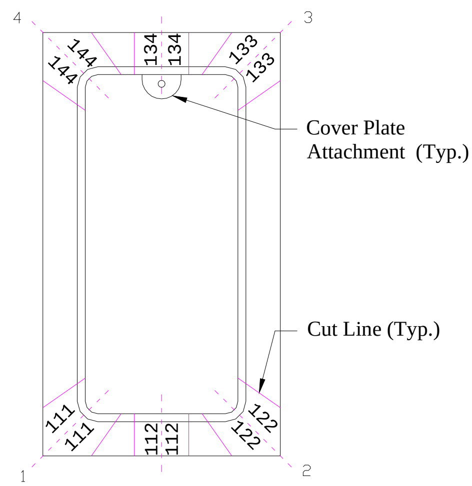

Figure 12.
Access Hole
Sample Location

The hand access hole sections were made in a similar manner, isolating the areas of maximum stress as discussed earlier. The sections shown in Figure 12 are through the corners and through the midpoint of the top and bottom sides of the hand access hole. In total 6 sections were made per hand access hole, resulting in total of 12 samples per hand access hole. The number system used for the hand access hole samples is also shown in Figure 12. The hand access holes of specimens B-1 through B-5 were sampled in this manner.

The exact location of maximum tensile stress of the complex corner style column to mast-arm connection is difficult to determine without detailed finite element analysis. As discussed earlier, the fabrication of these connections entails fillet welding both the perimeters of the slotted mast-arm and column to the oval plate and protruding internal diaphragm (Figure 4 and 5). According to simple beam theory, the portion of the fillet weld above the neutral axis will be subjected to tensile stress. The section of this weld identified to be most susceptible to fatigue crack growth was the weld between the mast-arm (as well as the column on the tension side) and the edge of the protruding internal diaphragm, marked in the photo in Figure 13.

Sections were taken through the center of the internal diaphragm where it was welded to the mast-arm, on the mast-arm side of the joint, and on the other side of the joint where the internal diaphragm was welded to the mast-arm, as shown previously in Figure 3 and 4. Sections were made of the welds between the internal diaphragm and both the column and mast-arm on the compression side also to gain a better understanding of the weld quality. Figure 13 shows the end of the internal diaphragm is fillet welded to the column/mast-arm. In the fabrication process, a small gap is introduced and then filled with weld material as discussed earlier. The section cuts directly through thickness of the internal diaphragm and the gap. Figure 14 shows an enlarged three dimensional view of a typical corner section sample. Figure 15 shows where sections were made, and the numbering convention used to identify the samples. For example, samples 61 and 62 are the tension samples, and 63 and 64 are the compression samples of specimen C-6.

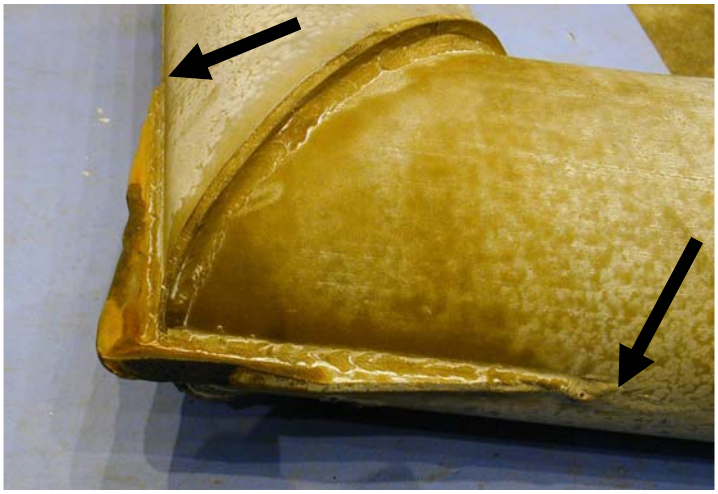

Figure 13. Section location of corner style column to mast-arm connection.

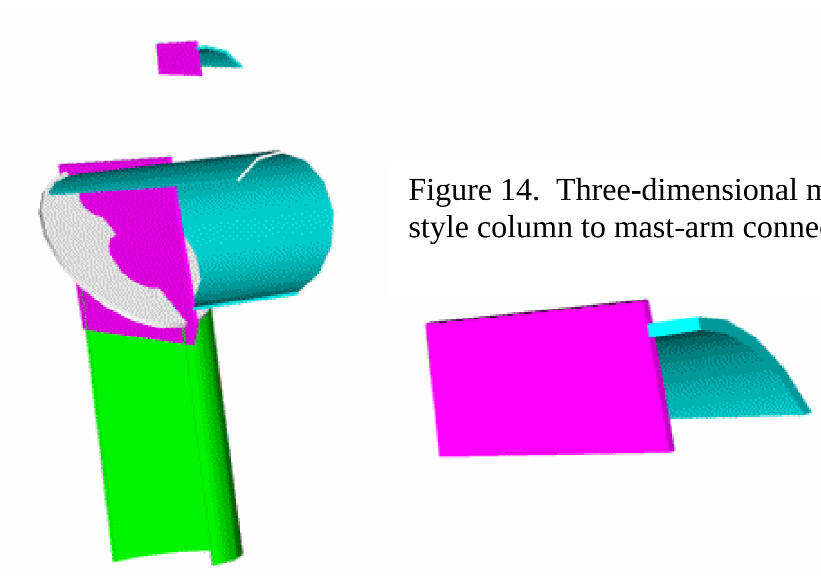

Figure 14. Three-dimensional model of corner style column to mast-arm connection and sample.

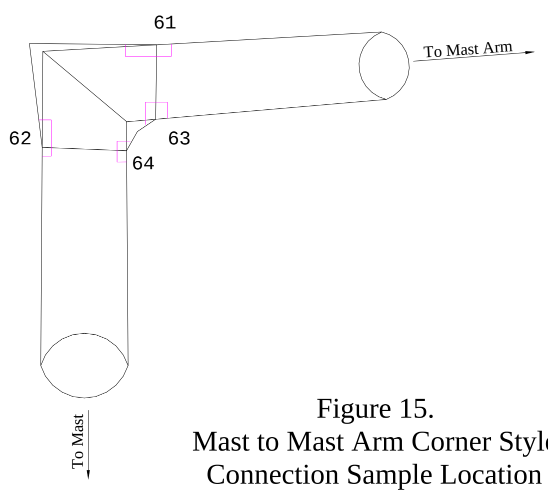

Figure 15.
Mast to Mast Arm Corner Style Connection Sample Location

Due to its similarity, the endplate specimen component of the endplate style column to mast-arm connection was sampled with the same exact procedure used in the baseplate specimens. The only difference was that the tension side of the endplate specimen did not have a hand access hole. The seam which identifies the bottom and hence the compression side of the mast-arm, was located on side 12, as seen in Figure 16. The endplate sections and sample numbering convention are shown in Figure 16 below also. Specimen E-9, the only endplate specimen obtained, was sampled according to this convention.

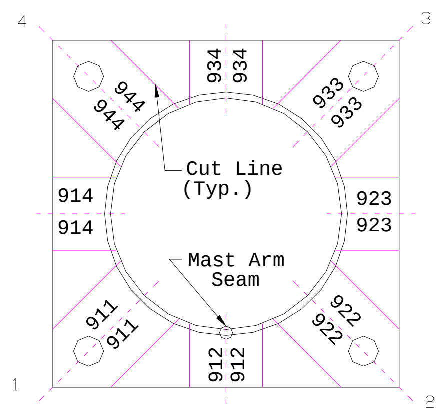

Figure 16.
Endplate Sample Locations

The built-up box specimen, specimen E-10, was sampled as indicated in Figure 17. The welded joints of the built-up box specimen can be divided into two groups, the welded joint between the flange plate, and the built-up box (samples 1, 2A, 2B, 3A, and 3B), the welded joint between the column and the built up box (samples 4-9) Samples 2A and 2B (as well as 3A and 3B) are two different one-sided samples. Sections were oriented consistent with the locations of maximum stress in the flange plate to built-up box connection. Hence, based on field measurements, sections were also located in line with the endplate bolts. But instead of taking samples of the weld at the corner of the flange plate, samples were taken just off the corner through the top of the built up box (samples 2A and 3A) and through the side of the built up box (samples 2B and 3B). The justification behind samples 4,5,7, and 8 again was that the maximum stress acts radially in line with the endplate bolts. Samples 7 and 8 are also areas in which previously documented fatigue investigations of cantilevered signal support structures have reported weld defects, which were suspected causes of failure. (Reference C)

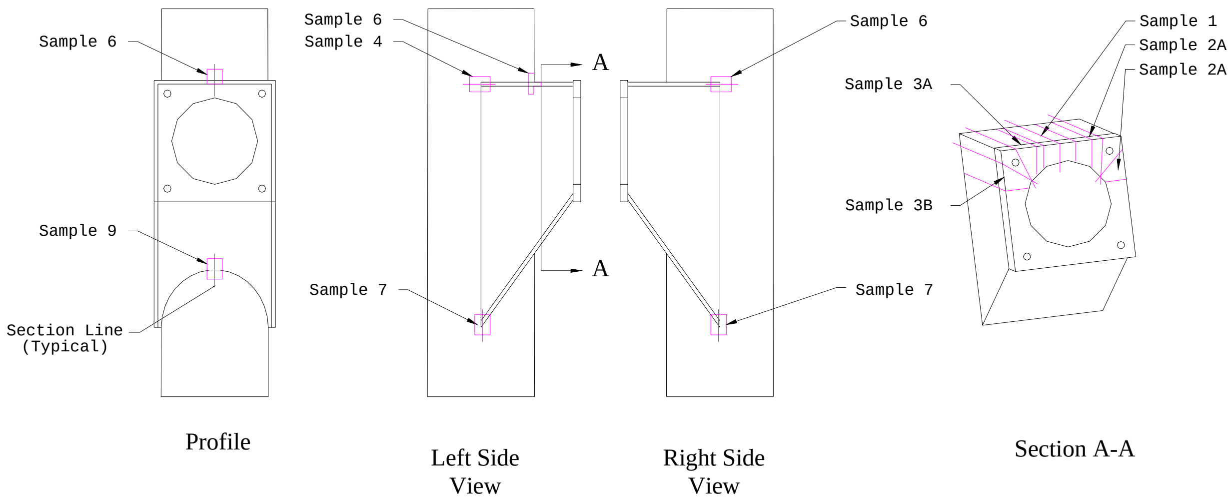

Figure 17. Sample locations of Built-up Box Specimen

B.5 Summary of Results

No fatigue cracks were identified in any of the cantilever signal support structure specimens provided by the city of Philadelphia. Overall weld quality of the specimens was fair to good in the context of mast-arm structures. Base plate to column weld details were overall very good with some minor weld defects. The end plate to mast-arm weld details were similarly in good condition. Hand access hole fillet welds were found to be very good. The welds between the internal diaphragms and the column and mast-arm of the corner style column to mast-arm connection were found to be of poor quality due to the difficulty in fabrication. The weld quality of the built-up box specimen was found to be good, with only minor weld defects present. The only types of weld defects detected in all of the specimens were the result of as fabricated incomplete penetration and lack of fusion. The following section describes the observations made on the weld quality of the various types of cantilevered signal support structures specimens obtained.

The hand access hole weld details showed no signs of fatigue cracking, and good fillet weld quality. Figure 18 shows a typical cross section through the hand access hole weld. Figure 19 is a photograph showing the relative high weld quality of the hand access hole weld. Note that the bottom portion shown in figure 19, is the cover plate attachment as shown in Figure 12.

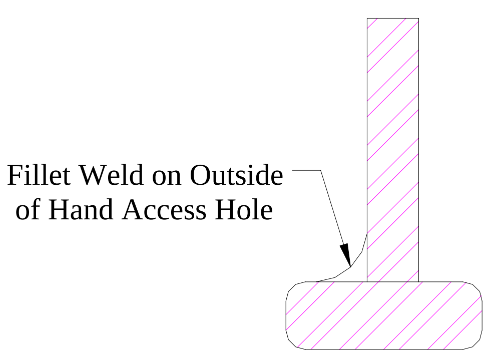

Figure 18. Typical hand access hole sample.

Figure 19. Hand Access Hole Sample.

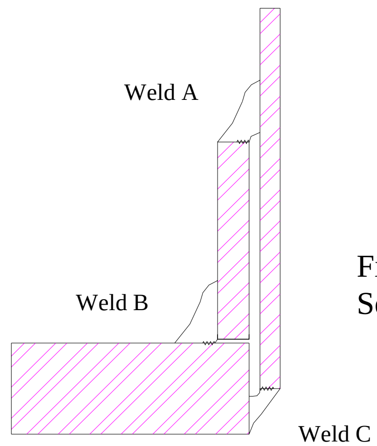

Figure 20. Sample Base Plate Section

The primary weld defects encountered in the base plate and end plate weld details were as fabricated incomplete fusion and inadequate joint penetration. A typical baseplate section is shown in Figure 20, indicating the three fillet welds, Weld A, Weld B, and Weld C, which make up the baseplate to column connection. (Note that Figure 20 applies equally to the typical end plate section.) The similarity between the end plate and base plate samples is illustrated in Figures 21 and 22.

Inadequate joint penetration implies that the weld metal fails to penetrate and bond all the way to the corner of the base metals of a welded joint. Several samples show that the weld metal of Welds A, B, and C did not fill the entire corner of the two adjoining base metals. Figures 21 and 22, which are photographs of base plate and end plate sample respectively, illustrate inadequate joint penetration. One common cause of inadequate joint penetration is poor joint geometry. The diameter of the electrode used in the welding process must be small enough to fill into the root of the weld, in this case, the corner of the two base metals. The majority of the samples contained evidence of small gaps between the base metal of the welded joints. The small gaps further complicate inadequate joint penetration. For example, in Weld B, a small vertical gap between the outer-ring and the base plate would often prevent the weld metal from bonding all the way to the root of the weld, because there was a gap in the corner formed by the base plate and outer-ring (As seen in Figure 21). The incomplete penetration would have very little affect on the structural strength performance of the joint, and very few samples showed a incomplete penetration that could be classified as poor weld quality. However inadequate joint penetration does have an affect on the fatigue behavior of welded joints, and will be discussed later.

Figure 21. Inadequate penetration in a baseplate sample (Weld B)

Figure 22. Inadequate penetration in an endplate sample (Weld B)

In addition to the inadequate joint penetration, the other type of weld defect present in the base plate and end plate weld details was an as fabricated lack of fusion or incomplete fusion. This weld defect was present in combination with inadequate joint penetration weld defects as well as by itself. As the name indicates a small portion of the fillet weld does not bond to fail to establish a bond to the base metal. Incomplete fusion weld defects are typically the result of improper surface pretreatment and insufficient welding current. Several samples showed this type of weld defect. As the fillet weld extends into the corner, it was common for the weld metal to lose its bond to the base metal. This defect looked very similar to a crack but occurred in both the horizontal and vertical legs of the fillet weld. Like the incomplete penetration discontinuities this weld defect was typically very small, and would have little affect on performance and weld quality. However lack of fusion discontinuities should be carefully differentiated between incomplete penetration discontinuities as they form sharper crack like discontinuities. Figures 23 and 24 show typical lack of fusion weld defects.

The examination of base plate samples showed a strong relation between inadequate penetration and incomplete fusion weld defects. Many samples indicated a combination of the two weld defects. As seen in Figure 24 a typical weld profile from the root to the toe of the weld consists of the following segments: Beginning at the tow is a segment void of weld metal which gradually tapers down until the weld metal makes contact, but does not bond with the base metal. This incomplete fusion segment was typically small and ended with a sharp point as the weld metal established a bond with the base metal. The final segment consisted of a complete bond between the weld metal and the base metal. As will be discussed later, by a fracture mechanics perspective, whether the weld defect is an incomplete fusion or inadequate penetration becomes irrelevant. The only necessary information is the total length of the defect and the sharpness of the point. It is worth noting the role geometric defects played in creating weld defects. A gap between the two base metals would oftentimes create a void or inadequate penetration in the weld metal. This void was oftentimes accompanied by a segment of incomplete fusion along the leg of the weld. When gaps were present in samples it was defect to be present rather than the weld metal to adequately penetrate into the gap.

Figure 23. Incomplete fusion weld defect

Figure 24. Combination inadequate penetration/incomplete fusion weld defect

Both incomplete penetration and lack of fusion are described in the American Welding Society as fusion type weld discontinuities. According to the AWS, weld discontinuities affect stresses in two ways. The first is that weld discontinuities, specifically lack of fusion, and incomplete penetration increase stress by reducing the nominal area of the weld. The most import affect these two weld discontinuities have on stress is due to the notch effect. Stress is concentrated at notch tips of cracks perpendicular to an applied tensile stress. The sharper the notch, the greater the stress concentration that is formed at the tip. Thus, incomplete fusion and inadequate penetration weld discontinuities concentrate stress at a point. Using a fracture mechanics approach, minimum stress ranges can be calculated for which fatigue cracks will initiate, or begin to form at the point where these discontinuities concentrate stress. The main significance of weld quality is that good weld quality minimizes these localized areas of concentrated stress. The American Welding Society's utilization of a functionality requirement in its definition of weld quality implies that weld quality should also include the fatigue performance of the weld. Because no fatigue damage was found, the weld quality of the base plate and end plate specimens obtained can be concluded as sufficient, according to the AWS stipulations. However, under more severe loading, fatigue cracks could develop.

Several of the welds examined from the corner style column to mast-arm connections were incomplete with gaps present in the weld material, occasionally penetrating the thickness of the weld. The presence of zinc inside of the lack of fusion weld discontinuities and coating these gaps clearly indicates that the weld discontinuities were formed during fabrication, not in service due to fatigue cracking. The lack of penetration of these welds can be seen in the Figures 25 and 26. Note the silvery zinc finish has actually penetrated through the weld during the anodization finishing process. The geometry of these joints made it very difficult to make a high quality weld between the internal diaphragm and the column or mast-arm. Several other of the samples indicated that this weld was made by haphazardly filling the gap with weld metal (See Figure 27).

The geometry of the corner style column to mast-arm connection likely allowed the stress alternate paths to transfer down into the column. Without a clear understanding of the stresses in these joints it is not possible to determine if the internal diaphragm to column/mast-arm weld was under maximum bending stress or whether the stress was reduced because the load followed an alternate load path. Fatigue crack initiation was not observed in areas of poor weld quality within the corner style column to mast-arm connection specimens obtained, even though one sample showed a complete gap in weld material. Judgment is necessary to conclude if the weld quality found, is sufficient, due to the many unknowns.

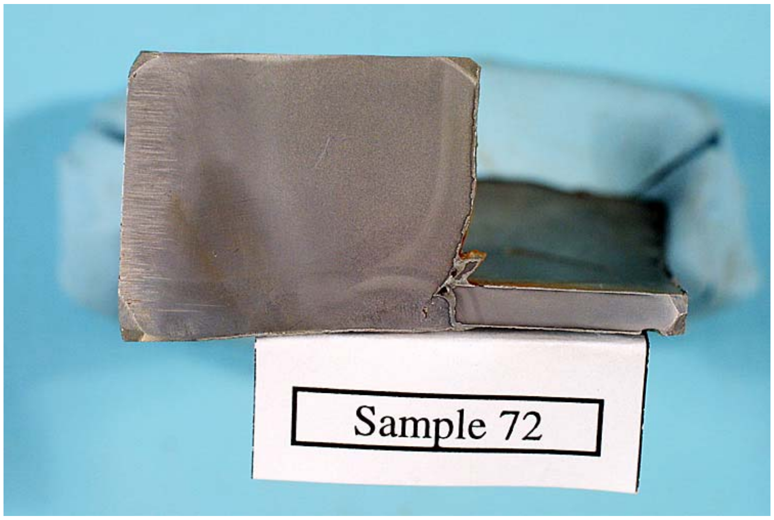

Figure 25. Corner style column to mast-arm connection sample. Note zinc finish penetrating through to the outer surface.

Figure 26. Corner style column to mast-arm connection sample. Note zinc finish inside the large weld metal gap.

Figure 27. Corner style column to mast-arm connection sample, showing the base metal gap filled in with a large amount of weld metal.

No fatigue cracks were found in the one built-up column specimen provided. The samples taken from the specimen indicated weld quality similar to the base plate specimens. Minor instances of as fabricated incomplete fusion and inadequate penetration weld defects were recorded. As previously discussed the geometry of the base metal had a strong influence on the resulting weld quality. As seen in Figure 28, a small gap in sample 3A results in an inadequate penetration and incomplete fusion weld defect. Several other minor incomplete fusion weld defects were recorded. This elevated occurrence of incomplete fusion weld defects as well as the visible incomplete fusion crack may suggest improper pre-weld surface preparation or may be the result of the difficult geometry of the built-up box weld details.

The crack found along the vertical fillet weld of the built-up box specimen was in no way the result of fatigue crack initiation. Instead the crack likely formed during errection, when the detail was loaded for the first time. Since there is no evidence of zinc inside the crack, it can be assumed that the crack was very small or partially fused together after fabrication. Sections were taken through and slightly above, the visible crack as seen in Figures 29 and 30. Both samples confirmed incomplete fusion and suggested that the crack formed in service as result of poor as fabricated fusion.

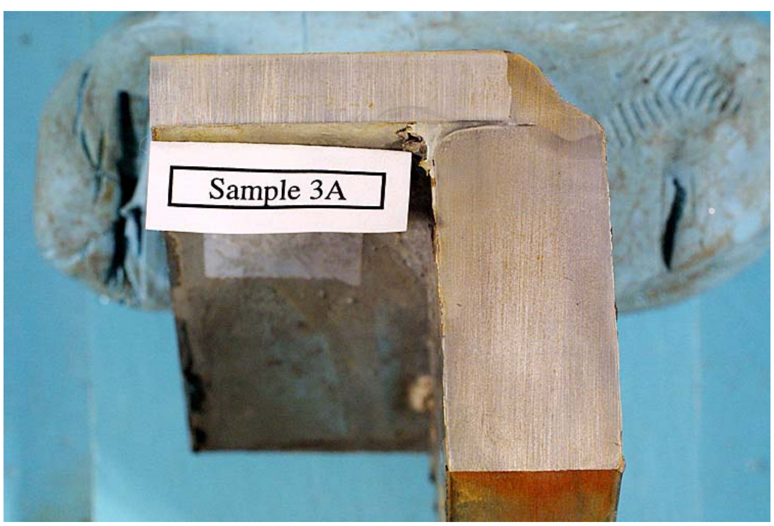

Figure 28. Built-up box sample 3A. Note the gap between base metals tapers into a sharp weld defect.

Figure 29. Built-up box sample 4. Note the incomplete fusion weld defect, a common defect fond in the built-up box samples.

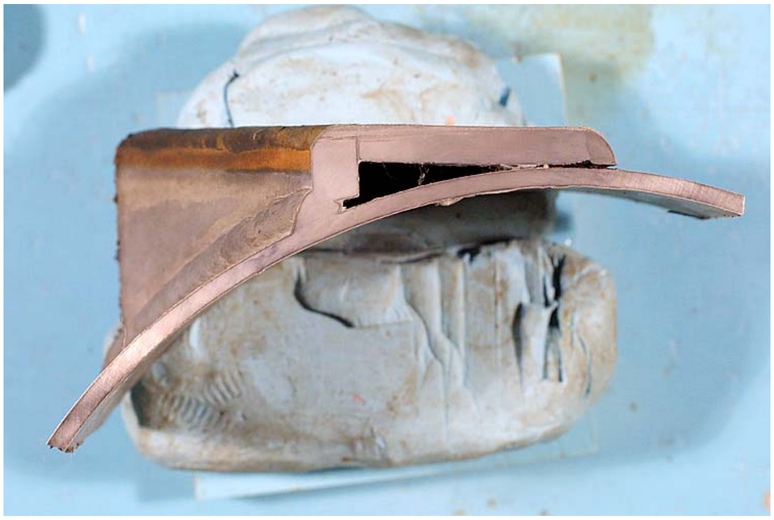

Figure 30. Section through vertical fillet weld crack. Note that there is no weld metal fusion within this section.

In conclusion, no fatigue cracks were found in any of the samples provided by the City of Philadelphia. Several locations where fatigue cracks would be expected to initiate were observed. These probable locations included lack of fusion and incomplete penetration weld discontinuities where stress concentrations are very high. Fracture Mechanics and advanced modeling can also be utilized to determine if fatigue cracks will initiate in the probable locations. Because the load histories are unknown for the specimens examined it is difficult to conclude whether or not to expect fatigue cracking in other similar structures. However the destructive evaluation of the specimens provides valuable insight to the weld quality of other similarly aged cantilevered signal support structures.

References

(A) American Association of State Highway & Transportation Officials, Standard Specifications for structural Supports for Highway Signs, Luminaires and Traffic Signals, AASHTO, 2001, 4th Edition.

(B) American Welding Society, Welding Handbook. Volume 1, 1987, 8th Edition

(C) Hamilton, H. R., Fowler T. J., Pucket J. A.. ASTM Special Technical Publication, Proceedings of the 1998 'Acoustic Emissions: Standards and Technology update' January 22-23 1998. Issue 1353, P 50-63 1999.